

Push–pull benzothiazole derivatives as probes for detecting b-amyloid plaques in Alzheimer's brains

Masahiro Ono^{a,*}, Shun Hayashi^a, Hiroyuki Kimura^a, Hidekazu Kawashima^b, Morio Nakayama^c, Hideo Saji^{a,*}

^a Graduate School of Pharmaceutical Sciences, Kyoto University, 46-29 Yoshida Shimoadachi-cho, Sakyo-ku, Kyoto 606-8501, Japan

^b Graduate School of Medicine, Kyoto University, Shogoin Kawahara-cho, Kyoto 606-8507, Japan

^c Graduate School of Biomedical Sciences, Nagasaki University, 1-14 Bunkyo-machi, Nagasaki 852-8521, Japan

article info

Article history:

Received 29 June 2009

Revised 4 August 2009

Accepted 4 August 2009

Available online 20 August 2009

Keywords:

β-Amyloid
Push–pull dye
Imaging
Alzheimer's disease

abstract

We synthesized push–pull benzothiazole derivatives and evaluated their potential as β-amyloid imaging probes. In binding experiments in vitro, the benzothiazoles showed excellent affinity for synthetic Aβ(1–42) aggregates. β-Amyloid plaques in the mouse and human brain were clearly visualized with the benzothiazoles, reflecting the results in vitro. These compounds may be a useful scaffold for the development of novel PET/SPECT and fluorescent tracers for detecting β-amyloid in Alzheimer's brains.

© 2009 Elsevier Ltd. All rights reserved.

1. Introduction

The formation of β-amyloid (Aβ) plaques is a key neurodegenerative event in Alzheimer's disease (AD).^{1,2} Since the imaging of these plaques in vivo may lead to the presymptomatic diagnosis of AD, many molecular probes for this purpose, including PET/SPECT and MRI tracers, have been developed.^{3–12} The PET ligand [¹¹C]-2-(4-(methylamino)phenyl)-6-hydroxybenzothiazole (6-OH-BTA-1 or PIB) with a benzothiazole backbone (Fig. 1) has shown particular promise in early clinical trials and is currently being used in a number of human studies.^{13–15} In addition to PET/SPECT and MRI probes, much attention has focused on the development of near-infrared fluorescent (NIRF) probes targeting Aβ plaques.^{16–18} NIRF probes are typically small molecule fluorescent dyes designed to absorb and emit light in the near-infrared region, where tissue scattering and absorption is lowest. The simple synthesis, low-cost, and long shelf-life of NIRF probes, together with the low-cost of optical imaging devices, present an attractive alternative to MRI and PET/SPECT techniques.

Among NIRF probes reported, to date, NIAD crosses the blood–brain barrier, selectively binds Aβ with high affinity, clears quickly

from the brain, and absorbs and emits within the near-infrared region (650–900 nm), often called the 'optical window' (Fig. 1).¹⁷ A series of NIAD derivatives have been designed and synthesized based on a classical push–pull architecture with terminal donor (hydroxy or dimethylamino group) and acceptor (dicyanomethylene group) moieties that are interconnected by a highly polarized bridge (dithienylethynyl group), because various donor and acceptor groups can be used to manipulate the relative energies of HOMO and LUMO and obtain the desired long wavelength of absorption/emission bands.¹⁷

On the basis of this approach to the molecular design, we planned to develop novel push–pull dyes for detecting Aβ plaques in the brain. We selected benzothiazole or styrylbenzothiazole as the highly polarized bridge, a dimethylamino group as the donor, and a dicyanomethylene group as the acceptor. In the present study, we designed and synthesized two benzothiazole-derived push–pull dyes (PP-BTA-1 and PP-BTA-2 in Fig. 2), and evaluated their biological potential as probes for detecting Aβ plaques in the brain. To our knowledge, this is the first time push–pull benzothiazole derivatives have been proposed as Aβ imaging probes for detecting AD.

2. Results and discussion

The target benzothiazole derivatives were prepared as shown in Schemes 1 and 2. PP-BTA-1 (4) was successfully synthesized in a yield of 21.4% according to methods reported previously (Scheme

* Corresponding authors. Tel.: +81 75 753 4608; fax: +81 75 753 4568 (M.O), tel.: +81 75 753 4556; fax: +81 75 753 4568 (H.S.).

E-mail addresses: ono@pharm.kyoto-u.ac.jp (M. Ono), hsaji@pharm.kyoto-u.ac.jp (H. Saji).

These authors contributed equally to this work.

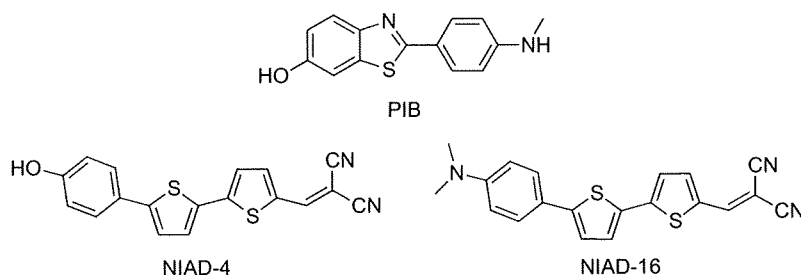


Figure 1. Chemical structures of PIB, NIAD-4 and NIAD-16.

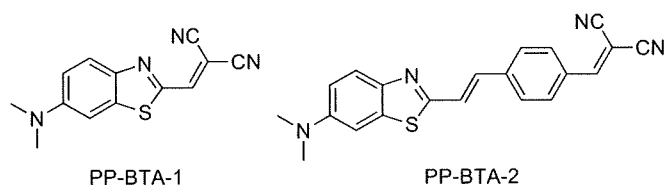


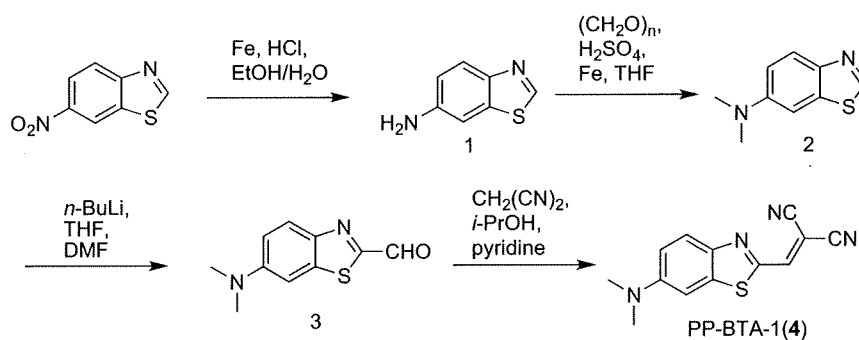
Figure 2. Chemical structures of push–pull benzothiazole derivatives reported in this paper.

1).¹⁹ The formation of styrylbenzothiazole in the synthesis of PP-BTA-2 (7) was achieved by a Wadsworth–Emmons reaction between diethyl (4-cyanobenzyl)phosphonate and 6-dimethylaminobenzothiazole-2-carbaldehyde. The desired (E)-styrylbenzothiazole derivative was prepared in a yield of 23.0%. The cyano group was converted to a formyl group by a reaction with DIBAL-H as reported.²⁰ The target PP-BTA-2 was prepared by the condensation of carbaldehyde with malononitrile.

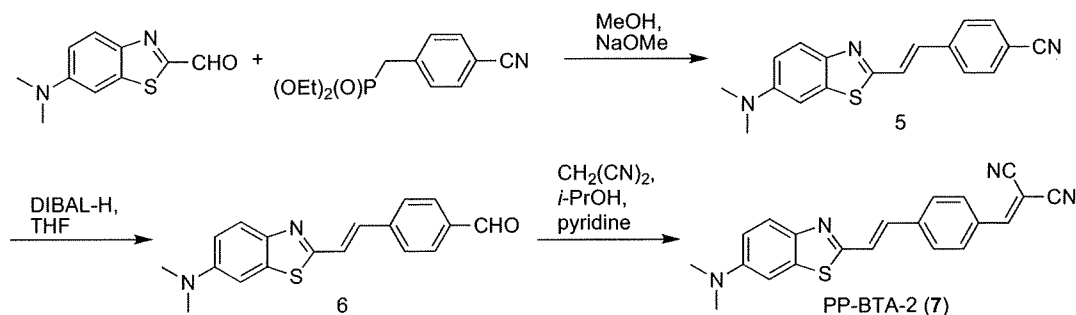
NIRF imaging in vivo requires the development of new fluorescent compounds with optimal fluorescent properties and high affinity for A β plaques. First, we evaluated the fluorescent proper-

ties (absorption/emission wavelengths) of PP-BTA-1 and PP-BTA-2. PP-BTA-1 and PP-BTA-2 exhibited absorption/emission peaks at 540/634 nm and 410/529 nm in EtOH, respectively. The extension of π -conjugation generally leads to absorption/emission bands with longer wavelengths. However, PP-BTA-2 showed a shorter wavelength than PP-BTA-1 despite a longer π -conjugation. On the other hand, because the wavelength of PP-BTA-1 is close to the near-infrared region, a slight modification should lead to a wavelength appropriate for imaging in vivo. Furthermore, when PP-BTA-1 and PP-BTA-2 existed in a solution containing A β (1-42) aggregates, the fluorescence intensity of PP-BTA-1 and PP-BTA-2 increased with the concentration of A β (1-42) aggregates, indicating affinity for A β aggregates (Fig. 3).

To quantify the affinity of push–pull benzothiazole derivatives for A β plaques, we carried out inhibition assays on the binding to A β (1-42) aggregates with thioflavin T as a competing ligand. PP-BTA-1 and PP-BTA-2 displaced thioflavin T in a dose-dependent manner, indicating that they have affinity for A β (1-42) aggregates (Fig. 4). In addition, this result suggests that PP-BTA-1 and PP-BTA-2 may occupy a binding site on A β aggregates similar to that of thioflavin T. The apparent IC₅₀ values for PP-BTA-1, PP-BTA-2 and PIB were 0.12, 0.11 and 0.67 μ M, respectively (Table 1). The IC₅₀ of



Scheme 1.



Scheme 2.

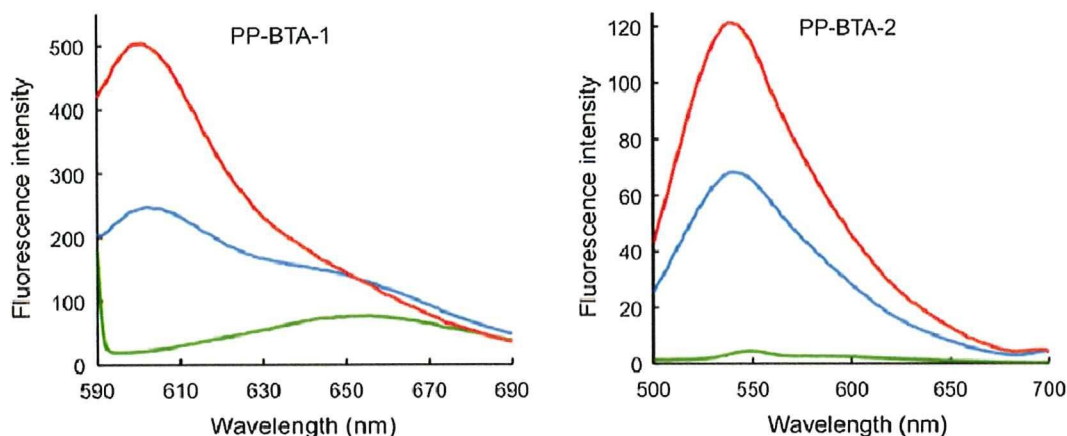


Figure 3. A β -dependent change in the fluorescence spectra of PP-BTA-1 and PP-BTA-2. Green, blue and red lines show the fluorescence spectrum of 0, 5 and 10 μ g/mL of A β (1-42) aggregates, respectively.

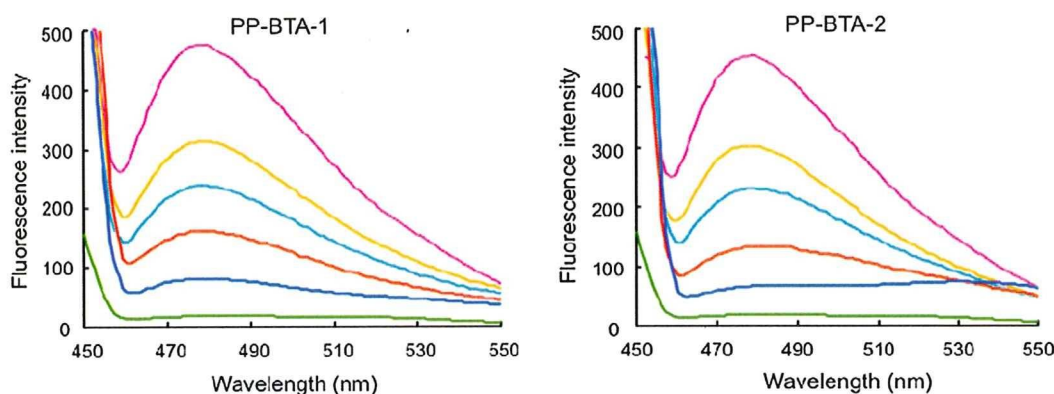


Figure 4. Inhibition assays of PP-BTA-1 and PP-BTA-2 using thioflavin T as the ligand in A β (1-42) aggregates. Fluorescence spectral change of thioflavin T (3 μ M) upon addition of 0.0611 (orange line), 0.122 (cyan line), 0.486 (red line), or 2.65 (blue line) μ M of PP-BTA-1 and PP-BTA-2 to A β (1-42) aggregates (10 μ g/mL). A pink line shows the fluorescence spectrum of thioflavin T (3 μ M) with A β (1-42) aggregates. A green line shows the fluorescence spectrum of thioflavin T (3 μ M) alone.

Table 1
Apparent inhibition constants (IC_{50} , μ M) of benzothiazoles for the binding of thioflavin T to A β (1-42) aggregates

Compound	IC_{50} ^a (μ M)
PP-BTA-1 (4)	0.12 \pm 0.001
PP-BTA-2 (7)	0.11 \pm 0.001
PIB	0.67 \pm 0.11

^a Each value represents the mean \pm standard error of the mean for three independent experiments.

PP-BTA-1 and PP-BTA-2 was lower than that of PIB, which is commonly used for clinical research, indicating PP-BTA-1 and PP-BTA-2 to have greater affinity for A β (1-42) aggregates. While PP-BTA-1 does not have the phenyl group in the phenylbenzothiazole structure that PIB possesses, it showed stronger binding to A β aggregates than PIB. Moreover, benzothiazole is a compact molecule advantageous for penetration of the blood–brain barrier after administration in vivo. These results suggest benzothiazole to be a useful scaffold for the development of A β imaging agents in vivo.

Next, the usefulness of PP-BTA-1 and PP-BTA-2 for neuropathological staining of A β plaques was investigated in an animal model of AD, the Tg2576 mouse, specifically engineered to overproduce A β plaques in the brain. PP-BTA-1 and PP-BTA-2 clearly stained the plaques as reflected by the high affinity for A β aggregates in in vitro competition assays (Fig. 5). The labeling pattern was consistent with that observed with thioflavin S. In contrast, wild-

type mice displayed no remarkable accumulation of PP-BTA-1 and PP-BTA-2 in brain sections. These results suggest that PP-BTA-1 and PP-BTA-2 show affinity for A β plaques in the mouse brain in addition to having affinity for synthetic A β (1-42) aggregates.

Furthermore, we also investigated the effectiveness of PP-BTA-1 and PP-BTA-2 for neuropathological staining of A β plaques in human AD brain sections (Fig. 6). A previous report suggested the configuration/folding of A β plaques in Tg2576 mice to be different from the tertiary/quaternary structure of A β plaques in AD brains.²¹ Therefore, it is important to evaluate the binding affinity for A β plaques in human AD brains. PP-BTA-1 and PP-BTA-2 clearly stained many neuritic plaques in AD brains (Fig. 6A and D). In contrast, no apparent staining was observed in adult normal brain sections (Fig. 6C and F). The labeling pattern was consistent with that observed by immunohistochemical labeling with an antibody specific to A β (Fig. 6B and E), indicating that PP-BTA-1 and PP-BTA-2 may be applicable for in vivo imaging of A β plaques in Alzheimer's brains and deserve further investigation as a potential tool for early diagnosis.

Since PP-BTA-1 and PP-BTA-2 possess a dimethylamino group, they can be used as probes for PET by labeling one of two methyl groups with ¹¹C. In addition, for the application of push–pull benzothiazole derivatives to optical imaging in vivo, the fine-tuning of absorption/emission wavelengths to a desired region continues by optimizing the combination of donor and acceptor groups.

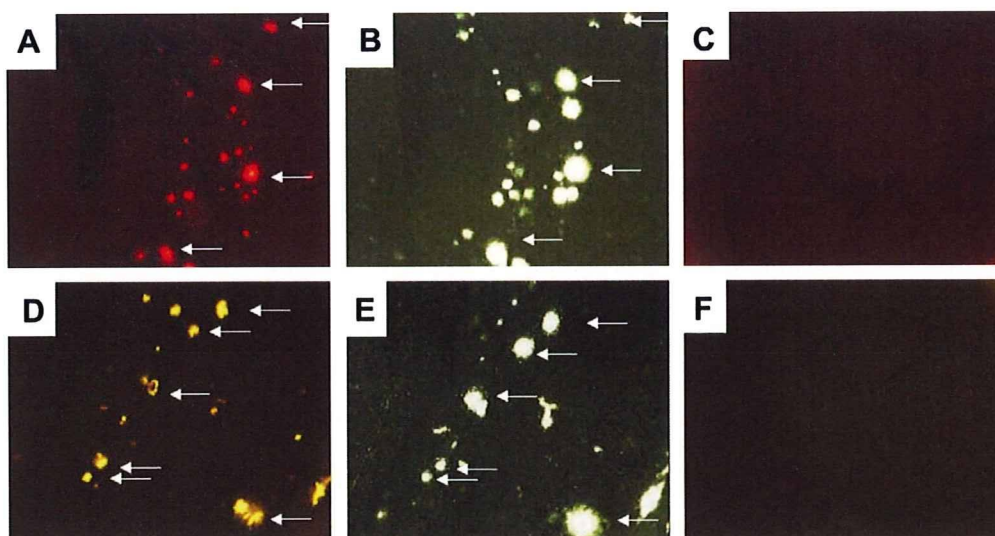


Figure 5. Neuropathological staining of PP-BTA-1 and PP-BTA-2 in 10 μm sections from a mouse model of AD (A and D) and a wild-type mouse (C and F). A β plaques labeled with PP-BTA-1 and PP-BTA-2 were confirmed by staining of the serial sections using thioflavin S (B and E).

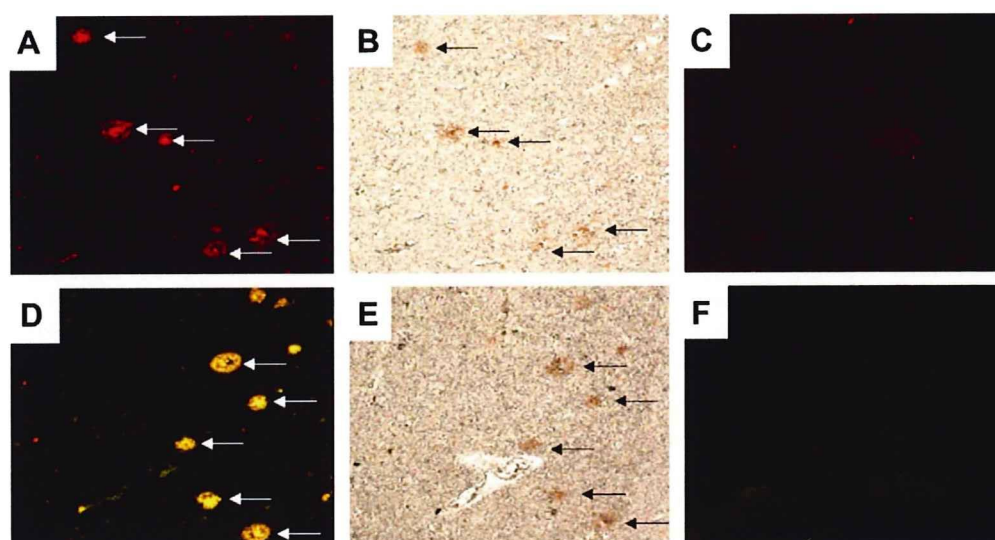


Figure 6. Neuropathological staining of 5 μm AD brain sections from the temporal cortex (A, B, D and E) and adult normal temporal brain sections (C and F). Many neuritic plaques are clearly stained with PP-BTA-1 (A) and PP-BTA-2 (D). Intense fluorescence can be seen in the core of neuritic plaques. A β immunostaining with anti A β antibodies in the serial sections shows an identical staining pattern of plaques (B and E). No apparent staining was observed in adult normal brain sections (C and F).

3. Conclusion

In conclusion, we successfully designed and synthesized benzothiazole-derived push–pull dyes for imaging A β plaques in the brain. In binding experiments *in vitro*, these benzothiazole compounds showed high affinity for A β (1–42) aggregates. PP-BTA-1 and PP-BTA-2 clearly stained A β plaques in both mouse brain and human brain, reflecting their affinity for A β aggregates *in vitro*. These findings suggest that additional structural changes on the benzothiazole backbone may be applied to potential A β probes for not only optical imaging but also PET and SPECT.

4. Experimental

^1H NMR spectra were obtained on a JEOL JNM-LM400 with TMS as an internal standard. Coupling constants are reported in hertz. Multiplicity was defined by s (singlet), d (doublet), t (triplet), br (broad) and m (multiplet). Mass spectra were obtained on a SHIMADZU LCMS-2010 EV. PIB was purchased from ABX (Radeberg,

Germany). Other reagents were of reagent grade and used without further purification unless otherwise indicated.

4.1. Chemistry

4.1.1. 1,3-Benzothiazol-6-amine (1)

To a mixture of 6-nitrobenzothiazole (2.5 g, 13.9 mmol) and concentrated HCl (1.93 mL, 22.7 mmol) in 80% EtOH (63 mL) was added powdered iron (3.7 g, 55.6 mmol). The reaction mixture was stirred for 1 h under reflux, and then cooled to room temperature. The precipitate of iron oxides and hydroxy salts was removed by filtration. The solvent was removed and the solid residue was extracted into a heterogeneous mixture of EtOAc (50 mL \times 2) and a 10% aqueous solution of Na $_2$ CO $_3$ (50 mL). The EtOAc extract was dried (Na $_2$ SO $_4$) and the solvent was removed under vacuum to yield 1 (1.91 g, 91.7%). ^1H NMR (400 MHz, CDCl $_3$) δ 8.70 (s, 1H), 7.89 (d, J = 8.8 Hz, 1H), 7.17 (d, J = 2.4 Hz, 1H), 6.87 (dd, J = 8.8, 2.4 Hz, 1H), 3.85 (br s, 2H). MS m/z 151 [MH $^+$].

4.1.2. N,N-Dimethyl-1,3-benzothiazol-6-amine (2)

A solution of 1 (1.47 g, 9.8 mmol) in THF (40 mL) was slowly added to a stirred mixture of 40% aqueous formaldehyde (7.24 mL, 98 mmol) and 4 M H₂SO₄ (7.95 mL, 29.4 mL). Powdered iron (4.36 g, 78.4 mL) was then added and the mixture was vigorously stirred for 3 h. The precipitate of iron salts was removed by filtration and washed with EtOAc (20 mL × 2). The combined organic solutions were made strongly basic with 1 N NaOH (50 mL) and extracted with EtOAc (50 mL × 2). The combined EtOAc extracts were dried (Na₂SO₄) and the solvent was removed on a rotary vacuum evaporator. The oily residue was purified by silica gel chromatography (hexane/EtOAc = 4:1) to give 2 (460 mg, 26.3%). ¹H NMR (400 MHz, CDCl₃) δ 8.67 (s, 1H), 7.95 (d, J = 8.8 Hz, 1H), 7.15 (d, J = 2.4 Hz, 1H), 7.00 (dd, J = 8.8, 2.4 Hz, 1H), 3.04 (s, 6H). MS m/z 179 [MH⁺].

4.1.3. 6-(Dimethylamino)-1,3-benzothiazole-2-carbaldehyde (3)

To a vigorously stirred solution of n-BuLi (0.5 mL, 2.6 M in hexane, 1.3 mmol) in THF (5.8 mL) at -78 °C under N₂ was added slowly a solution of 2 (220 mg, 1.23 mmol). The reaction mixture was stirred, warmed to -50 °C and after 1 h cooled to -78 °C. To the resulting solution of aryllithium salt was added slowly anhydrous DMF (0.38 mL). The solution was stirred for 2 h, poured into H₂O (9 mL), neutralized with an aqueous saturated solution of NH₄Cl and subsequently extracted with EtOAc (20 mL × 2). The combined extracts were dried over Na₂SO₄ and the solvent was removed under vacuum to give 3 (255 mg, 97.3%). ¹H NMR (400 MHz, CDCl₃) δ 10.06 (s, 1H), 8.03 (d, J = 10.0 Hz, 1H), 7.07–7.04 (m, 2H), 3.12 (s, 6H). MS m/z 207 [MH⁺].

4.1.4. ((6-(Dimethylamino)-1,3-benzothiazol-2-yl)methylene)malononitrile (PP-BTA-1, 4)

A solution of 3 (124 mg, 0.6 mmol), malononitrile (60 mg, 0.9 mmol) and pyridine (0.12 mL) in 2-propanol (7.2 mL) was stirred and refluxed for 30 min. The mixture was poured into H₂O (20 mL) and extracted with CHCl₃ (20 mL × 3). The combined extracts were dried over Na₂SO₄ and the solvent was removed under vacuum to give 4 (152 mg, 91.7%). ¹H NMR (400 MHz, CDCl₃) δ 7.99 (s, 1H), 7.99 (d, J = 9.2 Hz, 1H), 7.08 (dd, J = 9.2, 2.4 Hz, 1H), 7.02 (d, J = 2.4 Hz, 1H), 3.16 (s, 6H). MS m/z 255 [MH⁺]. Anal. Calcd for C₁₃H₁₀N₄S: C, 61.40; H, 3.96; N, 22.03; S, 12.61. Found: C, 61.34; H, 3.84; N, 21.82; S, 12.64.

4.1.5. 4-((E)-2-(6-(Dimethylamino)-1,3-benzothiazol-2-yl)vinyl)benzotrile (5)

To a solution of (4-cyanobenzyl)phosphonate (403.6 mg, 1.6 mmol) in MeOH (12.8 mL) was added NaOMe (0.632 mL). The mixture was cooled in an ice bath, and stirred under reflux for 3 h after the addition of 3 (330 mg, 1.6 mmol). The solid that formed in the reaction mixture was filtered to give 5 (385 mg, 78.8%). ¹H NMR (400 MHz, CDCl₃) δ 7.84 (d, J = 9.6 Hz, 1H), 7.64 (dd, J = 21.2, 8.0 Hz, 4H), 7.45 (d, J = 16.4 Hz, 1H), 7.32 (d, J = 16.4 Hz, 1H), 7.06 (d, J = 2.8 Hz, 1H), 6.95 (dd, J = 9.6, 2.8 Hz, 1H), 3.06 (s, 6H). MS m/z 306 [MH⁺].

4.1.6. 4-((E)-2-(6-(Dimethylamino)-1,3-benzothiazol-2-yl)vinyl)benzaldehyde (6)

To a solution of 5 (61 mg, 0.2 mmol) in THF (3.3 mL) was added DIBAL-H (1 M in hexane, 0.5 mL) at -78 °C. The reaction mixture was stirred at room temperature overnight. Thereafter, 10% acetic acid (15 mL) was added and the mixture was extracted with CHCl₃ (20 mL × 2). After the organic layer was washed with saline, the combined extracts were dried over Na₂SO₄. The residue was purified by silica gel chromatography (hexane/EtOAc = 2:1) to give 6 (28 mg, 45.4%). ¹H NMR (400 MHz, CDCl₃) δ 10.02 (s, 1H), 7.90 (d, J = 8.4 Hz,

2H), 7.85 (d, J = 8.2 Hz, 1H), 7.67 (d, J = 8.4 Hz, 2H), 7.50 (d, J = 16.4 Hz, 1H), 7.38 (d, J = 16.4 Hz, 1H), 7.07 (d, J = 2.4 Hz, 1H), 6.96 (dd, J = 8.8, 2.4 Hz, 1H), 3.06 (s, 6H). MS m/z 309 [MH⁺].

4.1.7. 4-((E)-2-(6-(Dimethylamino)-1,3-benzothiazol-2-yl)vinyl)benzylidene)malononitrile (PP-BTA-2, 7)

The same reaction as described above to prepare 5 was used, and 45 mg of 7 was obtained in a 63.5% yield from 6. ¹H NMR (400 MHz, CDCl₃) δ 7.94 (d, J = 8.4 Hz, 2H), 7.86 (d, J = 8.8 Hz, 1H), 7.73 (s, 1H), 7.68 (d, J = 8.4 Hz, 2H), 7.53 (d, J = 16.4 Hz, 1H), 7.35 (d, J = 16.4 Hz, 1H), 7.08 (s, 1H), 6.97 (d, J = 10.0 Hz, 1H), 3.08 (s, 6H). MS m/z 357 [MH⁺]. Anal. Calcd for C₂₁H₁₆N₄S: C, 70.76; H, 4.52; N, 15.72; S, 9.00. Found: C, 70.48; H, 4.57; N, 15.43; S, 8.99.

4.2. Fluorescence experiments

PP-BTA-1 and PP-BTA-2 were dissolved in 5% EtOH at 10 μM. The fluorescence of PP-BTA-1 and PP-BTA-2 was measured with a spectrophotometer (RF-1500, Shimadzu, Japan). For some measurements, the spectra of PP-BTA-1 and PP-BTA-2 were determined with or without Aβ(1-42) aggregates (0, 5 and 10 μM).

4.3. Binding experiments using Ab(1-42) aggregates

A solid form of Aβ(1-42) was purchased from Peptide Institute (Osaka, Japan). Aggregation was carried out by gently dissolving the peptide (0.25 mg/mL) in a buffer solution (pH 7.4) containing 10 mM sodium phosphate and 1 mM EDTA. The solution was incubated at 37 °C for 42 h with gentle and constant shaking. Thioflavin-T was used as the tracer for the competition binding experiments. A mixture (3.6 mL of 10% EtOH) containing PP-BTA-1, PP-BTA-2 and PIB (final concn 61.1 nM 5.48 μM), thioflavin-T (final concn 3 μM), and Aβ(1-42) aggregates (final concn 10 μg/mL) was incubated at room temperature for 10 min. Fluorescence intensity at an excitation wavelength of 445 nm was plotted, and values for the apparent half-maximal inhibitory concentration (IC₅₀) were determined from a calibration curve of fluorescence intensity at 478 nm in three independent experiments.

4.4. Staining of Ab plaques in Tg2576 mouse brain sections

The experiments with animals were conducted in accordance with our institutional guidelines and approved by the Kyoto University Animal Care Committee. The Tg2576 transgenic mice (female, 27-month-old) and wild-type mice (female, 27-month-old) were used as the Alzheimer's model and control mice, respectively. After the mice were sacrificed by decapitation, the brains were immediately removed and frozen in powdered dry ice. The frozen blocks were sliced into serial sections, 10 μm thick. Each slide was incubated with a 50% EtOH solution (100 μM) of PP-BTA-1 and PP-BTA-2 for 10 min. The sections were washed in 50% EtOH for 1 min two times, and examined using a microscope (Nikon Eclipse 80i) equipped with a G-2A filter set (excitation, 510–560 nm; dichroic mirror, 575 nm; longpass filter, 470 nm) for PP-BTA-1, and a B-2A filter set (excitation, 450–480 nm; dichroic mirror, 505 nm; longpass filter, 520 nm) for PP-BTA-2. Thereafter, the serial sections were also stained with thioflavin S, a pathological dye commonly used for staining Aβ plaques in the brain, and examined using a microscope (Nikon Eclipse 80i) equipped with a BV-2A filter set (excitation, 400–440 nm; dichroic mirror, 455 nm; longpass filter, 470 nm).

4.5. Staining of Ab plaques in human AD brain sections

Postmortem brain tissues from an autopsy-confirmed case of AD (73-year-old male) and a control subject (36-year-old male) were

obtained from BioChain Institute Inc. The sections were incubated with PP-BTA-1 and PP-BTA-2 (50% EtOH, 100 μ M) for 10 min at room temperature. The sections were washed in 50% EtOH for 1 min two times, and examined using a microscope (Nikon Eclipse 80i) equipped with a G-2A filter set (excitation, 510–560 nm; dichroic mirror, 575 nm; longpass filter, 470 nm) for PP-BTA-1, and a B-2A filter set (excitation, 450–480 nm; dichroic mirror, 505 nm; longpass filter, 520 nm) for PP-BTA-2. The presence and localization of plaques on the same sections were confirmed with immunohistochemical staining using a monoclonal A β antibody, BC05 (Wako).

Acknowledgements

This study was supported by the Program for Promotion of Fundamental Studies in Health Sciences of the National Institute of Biomedical Innovation (NIBIO), a Health Labour Sciences Research Grant, and a Grant-in-Aid for Young Scientists (A) and Exploratory Research from the Ministry of Education, Culture, Sports, Science and Technology, Japan.

References and notes

1. Klunk, W. E. *Neurobiol. Aging* 1998, 19, 145.
2. Selkoe, D. J. *Physiol. Rev.* 2001, 81, 741.
3. Shoghi-Jadid, K.; Small, G. W.; Agdeppa, E. D.; Kepe, V.; Ercoli, L. M.; Siddarth, P.; Read, S.; Satyamurthy, N.; Petric, A.; Huang, S. C.; Barrio, J. R. *Am. J. Geriatr. Psychiat.* 2002, 10, 24.
4. Mathis, C. A.; Wang, Y.; Holt, D. P.; Huang, G. F.; Debnath, M. L.; Klunk, W. E. *J. Med. Chem.* 2003, 46, 2740.
5. Ono, M.; Wilson, A.; Nobrega, J.; Westaway, D.; Verhoeff, P.; Zhuang, Z. P.; Kung, M. P.; Kung, H. F. *Nucl. Med. Biol.* 2003, 30, 565.
6. Klunk, W. E.; Engler, H.; Nordberg, A.; Wang, Y.; Blomqvist, G.; Holt, D. P.; Bergstrom, M.; Savitcheva, I.; Huang, G. F.; Estrada, S.; Ausen, B.; Debnath, M. L.; Barletta, J.; Price, J. C.; Sandell, J.; Lopresti, B. J.; Wall, A.; Koivisto, P.; Antoni, G.; Mathis, C. A.; Langstrom, B. *Ann. Neurol.* 2004, 55, 306.
7. Verhoeff, N. P.; Wilson, A. A.; Takeshita, S.; Trop, L.; Hussey, D.; Singh, K.; Kung, H. F.; Kung, M. P.; Houle, S. *Am. J. Geriatr. Psychiat.* 2004, 12, 584.
8. Small, G. W.; Kepe, V.; Ercoli, L. M.; Siddarth, P.; Bookheimer, S. Y.; Miller, K. J.; Lavretsky, H.; Burggren, A. C.; Cole, G. M.; Vinters, H. V.; Thompson, P. M.; Huang, S. C.; Satyamurthy, N.; Phelps, M. E.; Barrio, J. R. *N. Eng. J. Med.* 2006, 355, 2652.
9. Kudo, Y.; Okamura, N.; Furumoto, S.; Tashiro, M.; Furukawa, K.; Maruyama, M.; Itoh, M.; Iwata, R.; Yanai, K.; Arai, H. *J. Nucl. Med.* 2007, 48, 553.
10. Rowe, C. C.; Ackerman, U.; Browne, W.; Mulligan, R.; Pike, K. L.; O'Keefe, G.; Tochon-Danguy, H.; Chan, G.; Berlangieri, S. U.; Jones, G.; Dickinson-Rowe, K. L.; Kung, H. P.; Zhang, W.; Kung, M. P.; Skovronsky, D.; Dyrks, T.; Holl, G.; Krause, S.; Friebe, M.; Lehman, L.; Lindemann, S.; Dinkelborg, L. M.; Masters, C. L.; Villemagne, V. L. *Lancet. Neurol.* 2008, 7, 129.
11. Higuchi, M.; Iwata, N.; Matsuba, Y.; Sato, K.; Sasamoto, K.; Saido, T. C. *Nat. Neurosci.* 2005, 8, 527.
12. Poduslo, J. F.; Curran, G. L.; Peterson, J. A.; McCormick, D. J.; Fauq, A. H.; Khan, M. A.; Wengenack, T. M. *Biochemistry* 2004, 43, 6064.
13. Bacskai, B. J.; Frosch, M. P.; Freeman, S. H.; Raymond, S. B.; Augustinack, J. C.; Johnson, K. A.; Irizarry, M. C.; Klunk, W. E.; Mathis, C. A.; Dekosky, S. T.; Greenberg, S. M.; Hyman, B. T.; Growdon, J. H. *Arch. Neurol.* 2007, 64, 431.
14. Johnson, K. A.; Gregas, M.; Becker, J. A.; Kinnecom, C.; Salat, D. H.; Moran, E. K.; Smith, E. E.; Rosand, J.; Rentz, D. M.; Klunk, W. E.; Mathis, C. A.; Price, J. C.; Dekosky, S. T.; Fischman, A. J.; Greenberg, S. M. *Ann. Neurol.* 2007, 62, 229.
15. Pike, K. E.; Savage, G.; Villemagne, V. L.; Ng, S.; Moss, S. A.; Maruff, P.; Mathis, C. A.; Klunk, W. E.; Masters, C. L.; Rowe, C. C. *Brain* 2007, 130, 2837.
16. Hintersteiner, M.; Enz, A.; Frey, P.; Jaton, A. L.; Kinzy, W.; Kneuer, R.; Neumann, U.; Rudin, M.; Staufenberg, M.; Stoekli, M.; Wiederhold, K. H.; Gremlich, H. U. *Nat. Biotechnol.* 2005, 23, 577.
17. Nesterov, E. E.; Skoch, J.; Hyman, B. T.; Klunk, W. E.; Bacskai, B. J.; Swager, T. M. *Angew. Chem., Int. Ed. Engl.* 2005, 44, 5452.
18. Raymond, S. B.; Skoch, J.; Hills, I. D.; Nesterov, E. E.; Swager, T. M.; Bacskai, B. J. *Eur. J. Nucl. Med. Mol. Imaging* 2008, 35, S93.
19. Hrobarik, P.; Sigmundova, I.; Zahradnik, P. *Synthesis* 2005, 4, 600.
20. Cho, B. R.; Chajara, K.; Jung, H.; Son, K. H.; Jeon, S. J. *Org. Lett.* 2002, 4, 1703.
21. Toyama, H.; Ye, D.; Ichise, M.; Liow, J. S.; Cai, L.; Jacobowitz, D.; Musachio, J. L.; Hong, J.; Crescenzo, M.; Tipre, D.; Lu, J. Q.; Zoghbi, S.; Vines, D. C.; Seidel, J.; Katada, K.; Green, M. V.; Pike, V. W.; Cohen, R. M.; Innis, R. B. *Eur. J. Nucl. Med. Mol. Imaging* 2005, 32, 593.

Fluoro-pegylated Chalcones as Positron Emission Tomography Probes for in Vivo Imaging of β -Amyloid Plaques in Alzheimer's Disease

Masahiro Ono,^{*,†,‡} Rumi Watanabe,[†] Hidekazu Kawashima,[§] Yan Cheng,[‡] Hiroyuki Kimura,[‡] Hiroyuki Watanabe,[†] Mamoru Haratake,[†] Hideo Saji,[‡] and Morio Nakayama^{*,†}

[†]Department of Hygienic Chemistry, Graduate School of Biomedical Sciences, Nagasaki University, 1-14 Bunkyo-machi, Nagasaki 852-8521, Japan, [‡]Department of Patho-Functional Bioanalysis, Graduate School of Pharmaceutical Sciences, Kyoto University, Yoshida Shimoadachi-cho, Sakyo-ku, Kyoto 606-8501, Japan, and [§]Department of Nuclear Medicine and Diagnostic Imaging, Graduate School of Medicine, Kyoto University, Shogoin Kawahara-cho, Sakyo-ku, Kyoto 606-8507, Japan

Received July 16, 2009

This paper describes the synthesis and biological evaluation of fluoro-pegylated (FPEG) chalcones for the imaging of β -amyloid (A β) plaques in patients with Alzheimer's disease (AD). FPEG chalcone derivatives were prepared by the aldol condensation reaction. In binding experiments conducted in vitro using A β (1–42) aggregates, the FPEG chalcone derivatives having a dimethylamino group showed higher K_i values (20–50 nM) than those having a monomethylamino or a primary amine group. When the biodistribution of ¹¹C-labeled FPEG chalcone derivatives having a dimethylamino group was examined in normal mice, all four derivatives were found to display sufficient uptake for imaging A β plaques in the brain. ¹⁸F-labeled **7c** also showed good uptake by and clearance from the brain, although a slight difference between the ¹¹C and ¹⁸F tracers was observed. When the labeling of A β plaques was carried out using brain sections of AD model mice and an AD patient, the FPEG chalcone derivative **7c** intensely labeled A β plaques. Taken together, the results suggest **7c** to be a useful candidate PET tracer for detecting A β plaques in the brain of patients with AD.

Introduction

The formation of β -amyloid (A β^a) plaques is a key neurodegenerative event in Alzheimer's disease (AD).^{1,2} Because the imaging of A β plaques in vivo may lead to the presymptomatic diagnosis of AD, many radiotracers that bind to A β plaques have been developed.^{3,4} Preliminary reports of positron emission tomography (PET) suggested that the uptake and retention of 2-(4'-[¹¹C]methylaminophenyl)-6-hydroxybenzothiazole ([¹¹C]PIB, **1**)^{5,6} and 4-*N*-[¹¹C]methylamino-4'-hydroxystilbene ([¹¹C]SB-13, **2**)^{7,8} differed between the brain of AD patients and those of controls. However, because ¹¹C is a positron-emitting isotope with a $t_{1/2}$ of just 20 min, efforts are being made to develop comparable agents labeled with the isotope ¹⁸F ($t_{1/2}$ = 110 min). [¹⁸F]-2-(1-(2-(*N*-(2-fluoroethyl)-*N*-methylamino)naphthalene-6-yl)ethylidene)malononitrile ([¹⁸F]FDDNP, **3**)^{9,10} and [¹⁸F]-4-(*N*-methylamino)-4'-(2-(2-(2-fluoroethoxy)ethoxy)ethoxy)-stilbene ([¹⁸F]BAY94–9172, **4**)^{11,12} should be useful

as tracers for imaging A β plaques in the diagnosis of AD. Recent reports suggest that A β aggregates possess multiple ligand-binding sites, the density of which differs.^{13–15} Therefore, the development of novel probes that bind A β aggregates may lead to critical findings regarding the pathology of AD.

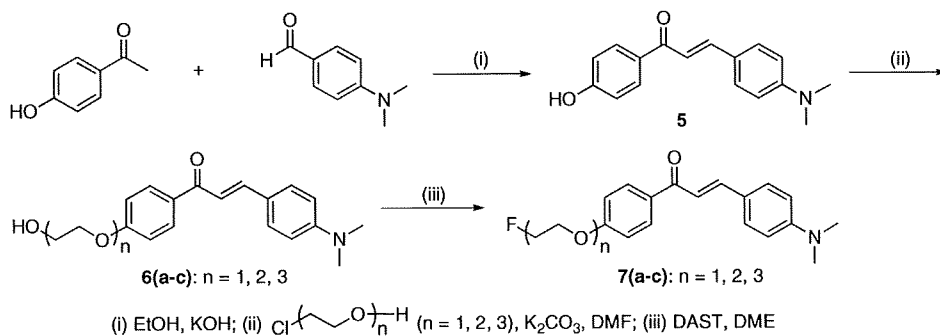
Recently, in a search for novel A β -imaging probes, we found that radioiodinated flavone,^{16,17} chalcone,^{18,19} and aurone^{20,21} derivatives, which are categorized as flavonoids, showed excellent characteristics such as high affinity for A β aggregates and good uptake into and rapid clearance from the brain. The chalcone structure in particular is considered to be a useful core in the development of new A β -imaging probes because it can be formed by a one-pot condensation reaction. In addition, because chalcone derivatives show different characteristics of binding to A β aggregates from Congo Red and thioflavin T, they are expected to provide new information from in vivo imaging in AD brains.

In the present study, we designed and synthesized fluorinated chalcone derivatives for the purpose of developing ¹⁸F-labeled probes for PET-based imaging of A β plaques. The formation of bioconjugates based on pegylation-fluorination resulting in fluoro-pegylated (FPEG) molecules is effective for some core structures of A β -imaging probes.²² We have adopted a novel approach, adding a short PEG (n = 1–3) to the chalcone backbone and capping the end of the ethylene glycol chain with a fluorine atom. Indeed, the most promising ¹⁸F-labeled agent **4** possesses PEG (n = 3) in the stilbene backbone. This tracer showed strong affinity (K_i = 6.7 nM) for A β plaques, high uptake (7.77%ID/g at 2 min postinjection), and rapid clearance from the mouse brain

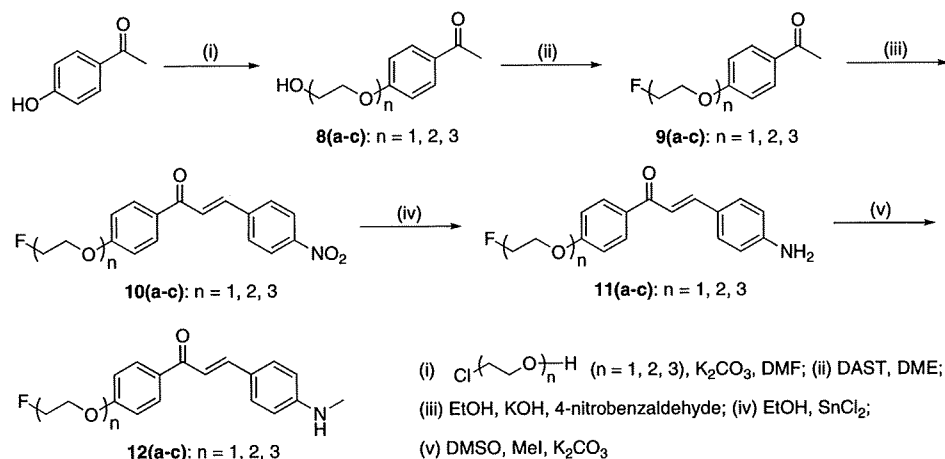
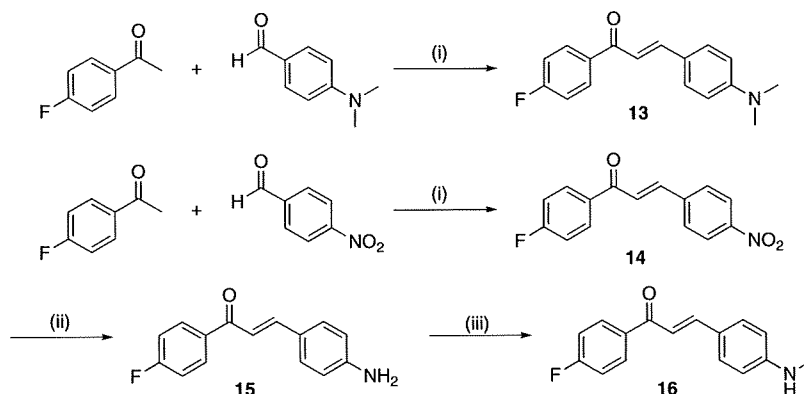
*To whom correspondence should be addressed. For M.O.: phone, +81-75-753-4608; fax, +81-75-753-4568; E-mail, ono@pharm.kyoto-u.ac.jp. For M.N.: phone, +81-95-819-2441; fax, +81-95-819-2441; E-mail: morio@nagasaki-u.ac.jp.

^a Abbreviations: A β , β -amyloid; AD, Alzheimer's disease; PET, positron emission tomography; PIB, 2-(4'-methylaminophenyl)-6-hydroxybenzothiazole; SB-13, 4-*N*-methylamino-4'-hydroxystilbene; FDDNP, 2-(1-(2-(*N*-(2-fluoroethyl)-*N*-methylamino)naphthalene-6-yl)ethylidene)malononitrile; BAY94-9172, 4-(*N*-methylamino)-4'-(2-(2-(2-fluoroethoxy)ethoxy)ethoxy)-stilbene; DMIC, 4-dimethylamino-4'-iodo-chalcone; IMPY, 6-iodo-2-(4'-dimethylamino)phenyl-imidazo[1,2-*a*]pyridine; FPEG, fluoro-pegylated; DAST, diethylamino sulfur trifluoride; DME, 1,2-dimethoxyethane; MEK, methyl ethyl ketone; [¹¹C]methyl triflate, [¹¹C]MeOTf; DAB, 3,3'-diaminobenzidine.

Scheme 1



Scheme 2

Scheme 3^a

^a (i) EtOH, KOH; (ii) EtOH, SnCl₂; (iii) DMSO, MeI, K₂CO₃.

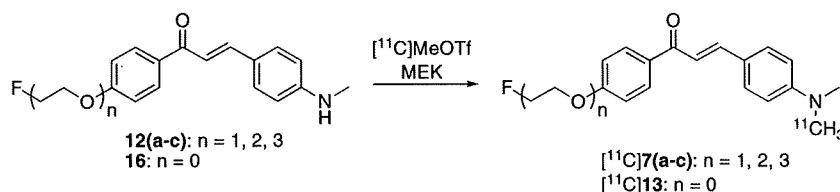
(1.61%ID/g at 60 min postinjection).¹² We adopted the biological data for **4** as criteria to develop novel A β -imaging agents. In this study, we synthesized 12 fluorinated chalcones and evaluated their biological potential as A β -imaging agents by testing their affinity for A β aggregates and A β plaques in sections of brain tissue from AD model mice and an AD patient and their uptake by and clearance from the brain in biodistribution experiments using normal mice.

Results and Discussion

The synthesis of the FPEG chalcone derivatives is outlined in Schemes 1, 2, and 3. The most useful way to prepare chalcones is the condensation of acetophenones with benzaldehydes. Using this process, 4-hydroxyacetophenone or

4-fluoroacetophenone was reacted with 4-dimethylaldehyde to form 4'-hydroxy-4-dimethylamino-chalcone **5** and 4'-fluoro-4-dimethylamino-chalcone **13** in yields of 84.0 and 41.6%, respectively. Compounds **10(a-c)** were synthesized by an aldol reaction between FPEG acetophenone **9(a-c)** and 4-nitrobenzaldehyde. Fluorination of **6(a-c)** and **8(a-c)** to prepare **7(a-c)** and **9(a-c)** was done using diethylamino sulfur trifluoride (DAST) after introducing three oligoethylene glycol molecules into the phenolic OH of **5** and **9(a-c)**. The amino derivatives **11(a-c)** and **15** were readily prepared from **10(a-c)** and **14** by reduction with SnCl₂. Conversion of **11(a-c)** and **15** to the monomethylamino derivatives **12(a-c)** and **16** was achieved by methylation with CH₃I under alkaline conditions. Preparation of ¹¹C-labeled compounds was done as in Scheme 4. ¹¹C-labeled chalcones

Scheme 4



Scheme 5

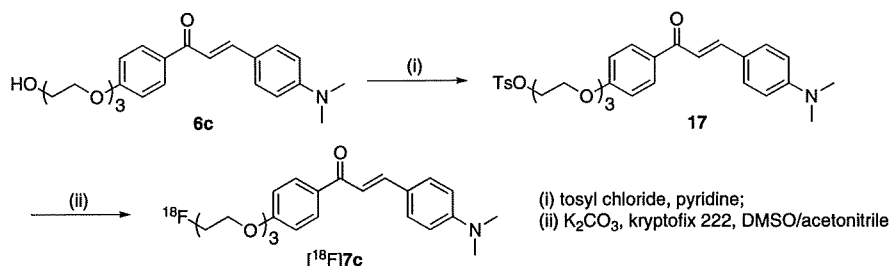
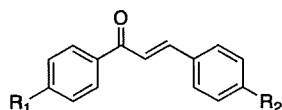


Table 1. Chemical Structures and Inhibition Constants of Fluorinated Chalcone Derivatives



compd	R ₁	R ₂	K _i (nM) ^a
7a	FCH ₂ CH ₂ O	N(CH ₃) ₂	45.7 ± 7.1
7b	F(CH ₂ CH ₂ O) ₂	N(CH ₃) ₂	20.0 ± 2.5
7c	F(CH ₂ CH ₂ O) ₃	N(CH ₃) ₂	38.9 ± 4.2
11a	FCH ₂ CH ₂ O	NH ₂	678.9 ± 21.7
11b	F(CH ₂ CH ₂ O) ₂	NH ₂	1048.0 ± 114.3
11c	F(CH ₂ CH ₂ O) ₃	NH ₂	790.0 ± 132.1
12a	FCH ₂ CH ₂ O	NHCH ₃	197.1 ± 58.8
12b	F(CH ₂ CH ₂ O) ₂	NHCH ₃	216.4 ± 13.8
12c	F(CH ₂ CH ₂ O) ₃	NHCH ₃	470.9 ± 100.4
13	F	N(CH ₃) ₂	49.8 ± 6.2
15	F	NH ₂	663.0 ± 88.3
16	F	NHCH ₃	234.2 ± 44.0
DMIC	I	N(CH ₃) ₂	13.1 ± 3.0
IMPY			28.0 ± 4.1

^aInhibition constants (K_i, nM) of compounds for the binding of [¹²⁵I]DMIC to Aβ(1–42) aggregates. Values are the mean ± standard error of the mean for 4–9 independent experiments.

were readily synthesized from their *N*-normethyl precursors, 12(a–c) and 16, and [¹¹C]methyl triflate ([¹¹C]-MeOTf). Radiochemical yields of the final product were 28–35%, decay corrected to end of bombardment. Radiochemical purity was >99% with a specific activity of 22–28 GBq/μmol. The identity of [¹¹C]7a, [¹¹C]7b, [¹¹C]7c, and [¹¹C]13 was confirmed by a comparison of HPLC retention times with the nonradioactive compounds (7a, 7b, 7c, and 13). ¹⁸F labeling of 7c was performed on a tosyl precursor 17 undergoing a nucleophilic displacement reaction with the fluoride anion (Scheme 5). Radiolabeling with ¹⁸F was successfully performed on the precursor to generate [¹⁸F]7c with a radiochemical yield of 45% and radiochemical purity >99%. The identity of [¹⁸F]7c was verified by a comparison of retention time with the nonradioactive compound. The specific activity of [¹⁸F]7c was estimated to be 35 GBq/mmol at the end of synthesis.

Table 2. Biodistribution of Radioactivity after Injection of [¹¹C]7a, [¹¹C]7b, [¹¹C]7c, and [¹¹C]13 in Normal Mice^a

organ	2 min	10 min	30 min	60 min
$[^{11}\text{C}]\text{7a}$				
blood	3.65 ± 0.37	2.73 ± 0.28	2.12 ± 0.18	2.22 ± 0.25
brain	6.01 ± 0.61	3.24 ± 0.39	2.57 ± 0.26	2.26 ± 0.41
$[^{11}\text{C}]\text{7b}$				
blood	3.48 ± 0.56	2.28 ± 0.84	2.54 ± 0.96	1.44 ± 0.36
brain	4.73 ± 0.47	2.23 ± 0.18	1.14 ± 0.12	1.00 ± 0.19
$[^{11}\text{C}]\text{7c}$				
blood	2.44 ± 0.25	1.52 ± 0.42	1.01 ± 0.15	0.68 ± 0.10
brain	4.31 ± 0.33	1.38 ± 0.16	0.64 ± 0.07	0.35 ± 0.03
$[^{11}\text{C}]\text{13}$				
blood	2.61 ± 0.35	1.60 ± 0.25	0.39 ± 0.05	1.40 ± 0.20
brain	3.68 ± 0.35	1.53 ± 0.14	1.04 ± 0.15	1.04 ± 0.20

^aExpressed as % of injected dose per gram. Each value represents the mean ± SD for 4–5 mice.

Table 3. Biodistribution of Radioactivity after Injection of [¹⁸F]7c in Normal Mice^a

organ	2 min	10 min	30 min	60 min
blood	2.09 ± 0.40	1.94 ± 0.18	2.35 ± 0.33	1.87 ± 0.26
brain	3.48 ± 0.47	1.52 ± 0.03	1.08 ± 0.09	1.07 ± 0.17
bone	1.80 ± 0.31	1.76 ± 0.15	2.98 ± 0.49	3.58 ± 0.41

^aExpressed as % of injected dose per gram. Each value represents the mean ± SD for 4–5 mice.

Experiments *in vitro* to evaluate the affinity of the FPEG chalcones for Aβ aggregates were carried out in solutions of Aβ aggregates with [¹²⁵I]4-dimethylamino-4'-iodo-chalcone ([¹²⁵I]DMIC)¹⁸ as the ligand (Table 1). The K_i values suggested that the binding to Aβ(1–42) aggregates was affected by substitution at the amino group at position 4 in the chalcone structure, not by the length of PEG introduced into the chalcone backbone. The fluorinated chalcones had binding affinity for Aβ(1–42) aggregates in the following order: the dimethylamino derivatives (7a, 7b, 7c, and 13) > the monomethylamino derivatives (12a, 12b, 12c, and 16) > the primary amino derivatives (11a, 11b, 11c, and 15). The result of the binding experiments is consistent with that of previous reports.^{16,19} In addition, the affinity of the dimethylamino

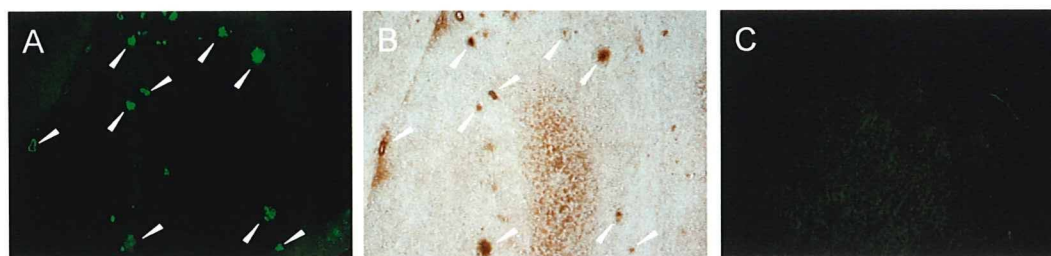


Figure 1. Neuropathological staining of 10 μm sections of a Tg2576 mouse brain (A and B) and aged normal brain (C). Fluorescent staining of compound **7c** in the Tg2576 mouse brain (A). A β immunostaining with antibody BC05 in the adjacent section (B). Fluorescent staining of compound **7c** in the age-matched control mouse brain (C).

derivatives was in the same range as that of the known compound, 6-iodo-2-(4'-dimethylamino)phenyl-imidazo[1,2-*a*]pyridine (IMPY), which is commonly used for inhibition assays.^{22–25} We selected the dimethylamino derivatives (**7a**, **7b**, **7c**, and **13**), which showed the greatest affinity, for additional studies.

To evaluate brain uptake of the FPEG chalcones, biodistribution experiments were performed in normal mice with four ¹¹C-labeled FPEG chalcones (¹¹C]**7a**, ¹¹C]**7b**, ¹¹C]**7c**, and ¹¹C]**13**) (Table 2). Because normal mice were used for the biodistribution experiments, no A β plaques were expected in the young mice; therefore the washout of probes from the brain should be rapid to obtain a higher signal-to-noise ratio earlier in the AD brain. Radioactivity after injection of the ¹¹C-labeled FPEG chalcones penetrated the blood–brain barrier, showing excellent uptake ranging from 3.7 to 6.0% ID/g brain at 2 min postinjection, a level sufficient for imaging A β plaques in the brain. In addition, they displayed good clearance from the normal brain with 2.3, 1.0, 0.35, and 1.0% ID/g at 60 min postinjection for ¹¹C]**7a**, ¹¹C]**7b**, ¹¹C]**7c**, and ¹¹C]**13**, respectively. These values were equal to 37.6, 21.1, 8.1, and 28.3% of the initial uptake peak for ¹¹C]**7a**, ¹¹C]**7b**, ¹¹C]**7c**, and ¹¹C]**13**, respectively. Compound **7c** with the fastest washout from the brain was labeled with ¹⁸F and evaluated for its biodistribution in normal mice (Table 3). [¹⁸F]**7c** displayed high uptake (3.48% ID/g) at 2 min postinjection, a level sufficient for imaging like ¹¹C]**7c**, and was cleared over the subsequent 10, 30, and 60 min. The radioactivity in the brain at 60 min postinjection was 1.07% ID/g, indicating that this [¹⁸F]**7c** has favorable pharmacokinetics in the brain. Although we consider that a slight difference of the radioactivity pharmacokinetics between ¹¹C]**7c** and [¹⁸F]**7c** could be attributable to the different physicochemical characteristics of their radiometabolites produced in the brain, the reason for this difference has remained unclear. Bone uptake at 60 min was measurable (3.58% ID/g), suggesting defluorination in vivo. Bone uptake has been observed for other ¹⁸F tracers.^{12,22–24} However, previous reports suggested that free fluoride was not taken up by brain tissue; therefore, the interference from free fluoride may be relatively low for brain imaging. A previous paper regarding the most promising ¹⁸F-labeled agent **4** reported that it showed high uptake (7.77% ID/g at 2 min postinjection) and rapid clearance from the brain (1.61% ID/g at 60 min postinjection) with little accumulation in bone (1.77% ID/g at 60 min postinjection) in biodistribution experiments using normal mice.¹² The pharmacokinetics of **4** appear superior to that of [¹⁸F]**7c**, but the good biological results obtained with [¹⁸F]**7c** suggest that further investigation is warranted.

To investigate the ability of the fluorinated chalcones to bind to A β plaques in the AD model, fluorescent staining of

sections of mouse brain were carried out with compound **7c** (Figure 1). We used Tg2576 transgenic mice as an animal model of A β plaque deposition, which express human APP695 with the K670N, M671L Swedish double mutation.²⁶ By 11–13 months of age, Tg2576 mice show prominent A β deposition in the cingulate cortex, entorhinal cortex, dentate gyrus, and CA1 hippocampal subfield and have been frequently used for the evaluation of specific binding of A β plaques in in vitro and in vivo experiments.^{12,24,27–31} Many A β plaques were clearly stained with **7c**, as reflected by the affinity for the aggregates of synthetic A β (1–42) in in vitro competition assays (Figure 1A). The labeling pattern was consistent with that observed after immunohistochemical labeling by BC05, a specific antibody for A β (Figure 1B), while wild-type mouse brain displayed no significant accumulation of **7c** (Figure 1C). The results indicated that **7c** binds specifically to A β plaques in Tg2576 mice brain. A previous report suggested the configuration/folding of A β plaques in Tg2576 mice to be different from the tertiary/quaternary structure of A β plaques in AD brains.^{30,32} In addition, the studies reported with **1** further indicate that the binding of **1** reflects the amount of A β plaques in human AD brain but not in Tg2576 mouse brain, and the detectability of A β plaques by **1** is dependent on the accumulation of specific A β subtypes.^{28,29} Therefore, we considered that it should be essential to evaluate the binding affinity for A β plaques in human AD brains because our goal is to develop clinically useful probes for in vivo imaging of A β plaques in humans.

Next, we investigated the binding affinity of [¹⁸F]**7c** for A β plaques by in vitro autoradiography in a human AD brain section (Figure 2A). The autoradiographic image of [¹⁸F]**7c** showed high levels of radioactivity in some specific areas of the brain section. Furthermore, we confirmed that the hot spots of [¹⁸F]**7c** in an AD brain section corresponded with those of in vitro thioflavin-S staining in the same brain section (Figure 2B). In contrast, no significant accumulation of [¹⁸F]**7c** was observed in the region without A β plaques (Figure 2C). The results demonstrate the feasibility of using [¹⁸F]**7c** as a probe for detecting A β plaques in the brain of AD patients with PET.

In conclusion, we reported novel FPEG chalcone derivatives, containing an end-capped fluoropolyethylene glycol as in vivo PET imaging agents for A β plaques in the brain. The FPEG chalcones with a dimethylamino group displayed greater affinity for synthetic A β aggregates than did the monomethylamino and primary amino derivatives. In biodistribution experiments using normal mice, ¹¹C-labeled FPEG chalcones displayed sufficient uptake for the imaging of A β plaques in the brain. ¹¹C]**7c** showed the fastest clearance from the brain, probably related to a low nonspecific binding. [¹⁸F]**7c** also displayed high uptake in and good clearance from

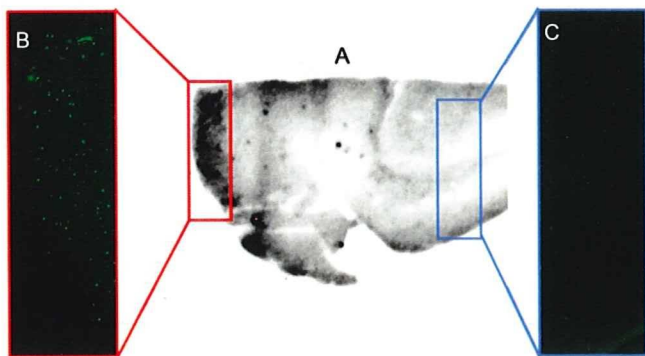


Figure 2. In vitro autoradiography of [^{18}F]7c using the human AD brain section (A). A β plaques were confirmed by in vitro staining of the same section with thioflavin-S (B and C).

the brain, although a slight difference was observed between the ^{11}C and ^{18}F tracers. When the labeling of plaques in vitro was carried out using sections of brain tissue from an animal model of AD and an AD patient, compound 7c intensely labeled A β plaques existing in both brains. Taken together, the results suggest the novel FPEG chalcone 7c to be potentially useful for imaging A β plaques in the brain using PET.

Experimental Section

General. All reagents were obtained commercially and used without further purification unless otherwise indicated. ^1H NMR spectra were obtained on a Varian Gemini 300 spectrometer with TMS as an internal standard. Coupling constants are reported in hertz. Multiplicity was defined by s (singlet), d (doublet), t (triplet) and m (multiplet). Mass spectra were obtained on a JEOL IMS-DX instrument. HPLC analysis was performed on a Shimadzu HPLC system (a LC-10AT pump with a SPD-10A UV detector, $\lambda = 254$ nm) using a Cosmosil C $_{18}$ column (Nakalai Tesque, 5C $_{18}$ -AR-II, 4.6 mm \times 150 mm) using acetonitrile/water (50/50) as mobile phase at a flow rate of 1.0 mL/min. All key compounds were proven by this method to show $\geq 95\%$ purity.

Chemistry. (*E*)-3-(4-(Dimethylamino)phenyl)-1-(4-hydroxyphenyl)-2-propen-1-one (5). 4-Hydroxyacetophenone (1.36 g, 10 mmol) and 4-dimethylaminobenzaldehyde (1.86 g, 10.0 mmol) were dissolved in EtOH (15 mL). A 30 mL aliquot of a 10% aqueous KOH solution was then slowly added dropwise to the reaction mixture. The mixture was stirred for 24 h at 100 $^\circ\text{C}$ and then extracted with ethyl acetate. After the organic layers were combined and dried over Na_2SO_4 , evaporation of the solvent afforded 1.50 g of 5 (84.0%). ^1H NMR (CD_3OD) δ : 3.04 (s, 6H), 6.76 (d, $J = 8.7$ Hz, 2H), 6.88 (d, $J = 8.7$ Hz, 2H), 7.50 (d, $J = 15.3$ Hz, 1H), 7.59 (d, $J = 9.0$ Hz, 2H), 7.72 (d, $J = 15.3$ Hz, 1H), 7.98 (d, $J = 8.7$ Hz, 2H). ^1H NMR ($\text{DMSO}-d_6$) δ : 2.99 (s, 6H), 6.74 (d, $J = 8.7$ Hz, 2H), 6.88 (d, $J = 8.4$ Hz, 2H), 7.62 (s, 2H), 7.68 (d, $J = 8.7$ Hz, 2H), 8.03 (d, $J = 8.7$ Hz, 2H), 10.30 (s, 1H). EI-MS: m/z 267 (M^+).

(*E*)-3-(4-(Dimethylamino)phenyl)-1-(4-(2-hydroxyethoxy)phenyl)-2-propen-1-one (6a). To a solution of 5 (500 mg, 1.87 mmol) and ethylene chlorohydrin (125 μL , 1.87 mmol) in DMSO (5 mL) was added anhydrous K_2CO_3 (775 mg, 5.61 mmol). The reaction mixture was stirred for 18 h at 100 $^\circ\text{C}$ and then poured into water and extracted with chloroform. The organic layers were combined and dried over Na_2SO_4 . Evaporation of the solvent afforded a residue, which was purified by silica gel chromatography (hexane: ethyl acetate = 1:1) to give 422 mg of 6a (72.7%). ^1H NMR (CDCl_3) δ : 3.04 (s, 6H), 4.00–4.01 (m, 2H), 4.17 (t, $J = 4.8$ Hz, 2H), 6.69 (d, $J = 9.0$ Hz, 2H), 6.99 (d, $J = 6.9$ Hz, 2H), 7.35 (d, $J = 15.3$ Hz, 1H), 7.55 (d, $J = 9.0$ Hz, 2H), 7.79 (d, $J = 15.3$ Hz, 1H), 8.02 (d, $J = 9.3$ Hz, 2H).

(*E*)-3-(4-(Dimethylamino)phenyl)-1-(4-(2-(hydroxyethoxy)ethoxy)phenyl)-2-propen-1-one (6b). The reaction described above to prepare 6a was used, and 6b was obtained from 5 and ethylene glycol mono-2-chloroethyl ether. ^1H NMR (CDCl_3) δ : 3.05 (s, 6H), 3.69 (t, $J = 4.8$ Hz, 2H), 3.78 (s, 2H), 3.91 (t, $J = 4.8$ Hz, 2H), 4.23 (t, $J = 4.8$ Hz, 2H), 6.70 (d, $J = 9.0$ Hz, 2H), 6.99 (d, $J = 9.0$ Hz, 2H), 7.35 (d, $J = 15.3$ Hz, 1H), 7.55 (d, $J = 8.7$ Hz, 2H), 7.79 (d, $J = 15.6$ Hz, 1H), 8.02 (d, $J = 9.0$ Hz, 2H).

(*E*)-3-(4-(Dimethylamino)phenyl)-1-(4-(2-(hydroxyethoxy)ethoxy)phenyl)-2-propen-1-one (6c). The reaction described above to prepare 6a was used, and 429 mg of 6c was obtained in a yield of 82.6% from 5 and 2-[2-(2-chloroethoxy)ethoxy]ethanol. ^1H NMR (CDCl_3) δ : 3.04 (s, 6H), 3.62 (t, $J = 5.1$ Hz, 2H), 3.73–3.75 (m, 6H), 3.90 (t, $J = 4.8$ Hz, 2H), 4.22 (t, $J = 4.8$ Hz, 2H), 6.70 (d, $J = 9.0$ Hz, 2H), 6.99 (d, $J = 8.7$ Hz, 2H), 7.35 (d, $J = 15.3$ Hz, 1H), 7.55 (d, $J = 9.0$ Hz, 2H), 7.78 (d, $J = 15.3$ Hz, 1H), 8.02 (d, $J = 9.0$ Hz, 2H).

(*E*)-3-(4-(Dimethylamino)phenyl)-1-(4-(2-(fluoroethoxy)phenyl)-2-propen-1-one (7a). To a solution of 6a (100 mg, 0.32 mmol) in 1,2-dimethoxyethane (DME) (5 mL) was added DAST (85 μL , 0.64 mmol) in a dry ice–acetone bath. The reaction mixture was stirred for 1 h at room temperature and then poured into a saturated NaHSO_3 solution and extracted with chloroform. After the organic phase was separated, dried over Na_2SO_4 , and filtered, and the residue was purified by preparative TLC (hexane:ethyl acetate = 3:1) to give 39 mg of 7a (38.9%). ^1H NMR (CDCl_3) δ : 3.09 (s, 6H), 4.30 (d, t, $J_1 = 27.6$ Hz, $J_2 = 4.2$ Hz, 2H), 4.79 (d, t, $J_1 = 47.4$ Hz, $J_2 = 4.2$ Hz, 2H), 6.70 (d, $J = 8.7$ Hz, 2H), 7.00 (d, $J = 9.0$ Hz, 2H), 7.35 (d, $J = 15.6$ Hz, 1H), 7.55 (d, $J = 9.0$ Hz, 2H), 7.79 (d, $J = 15.3$ Hz, 1H), 8.03 (d, $J = 9.0$ Hz, 2H). EI-MS: m/z 313 (M^+).

(*E*)-3-(4-(Dimethylamino)phenyl)-1-(4-(2-(fluoroethoxy)ethoxy)phenyl)-2-propen-1-one (7b). The reaction described above to prepare 7a was used, and 28 mg of 7b was obtained in a yield of 28.0% from 6b. ^1H NMR (CDCl_3) δ : 3.04 (s, 6H), 3.77–3.94 (m, 4H), 4.21–4.24 (m, 3H), 4.61 (d, t, $J_1 = 47.4$ Hz, $J_2 = 4.2$ Hz, 1H), 6.69 (d, $J = 9.3$ Hz, 2H), 6.99 (d, $J = 8.7$ Hz, 2H), 7.35 (d, $J = 15.3$ Hz, 2H), 7.55 (d, $J = 9.0$ Hz, 2H), 7.78 (d, $J = 15.6$ Hz, 2H), 8.02 (d, $J = 9.0$ Hz, 2H). EI-MS: m/z 357 (M^+).

(*E*)-3-(4-(Dimethylamino)phenyl)-1-(4-(2-(fluoroethoxy)ethoxy)ethoxy)phenyl)-2-propen-1-one (7c). The reaction described above to prepare 7a was used, and 29 mg of 7c was obtained in a yield of 14.4% from 6c and 2-[2-(2-chloroethoxy)ethoxy]ethanol. ^1H NMR (CDCl_3) δ : 3.04 (s, 6H), 3.73–3.81 (m, 6H), 3.90 (t, $J = 5.1$ Hz, 2H), 4.21 (t, $J = 5.1$ Hz, 2H), 4.49 (t, $J = 4.5$ Hz, 1H), 4.65 (t, $J = 4.5$ Hz, 1H), 6.70 (d, $J = 8.7$ Hz, 2H), 6.98 (d, $J = 9.0$ Hz, 2H), 7.35 (d, $J = 15.3$ Hz, 1H), 7.55 (d, $J = 8.7$ Hz, 2H), 7.78 (d, $J = 15.3$ Hz, 1H), 8.02 (d, $J = 9.0$ Hz, 2H). EI-MS: m/z 401 (M^+).

1-(4-(2-Hydroxyethoxy)phenyl)ethanone (8a). The reaction described above to prepare 6a was used, and 1.79 g of 8a was obtained in a yield of 99.4% from 4-hydroxyacetophenone and ethylene chlorohydrin. ^1H NMR (CDCl_3) δ : 2.75 (s, 3H), 4.20 (s, 2H), 4.35 (t, $J = 5.1$ Hz, 2H), 7.15 (d, $J = 9.0$ Hz, 2H), 8.13 (d, $J = 9.0$ Hz, 2H).

1-(4-(2-(2-Hydroxyethoxy)ethoxy)phenyl)ethanone (8b). The reaction described above to prepare 6b was used, and 8b was obtained from 4-hydroxyacetophenone and ethylene glycol mono-2-chloroethyl ether. ^1H NMR (CDCl_3) δ : 2.56 (s, 3H), 3.68 (t, $J = 4.8$ Hz, 2H), 3.75–3.79 (m, 2H), 3.90 (t, $J = 5.1$ Hz, 2H), 4.21 (t, $J = 4.8$ Hz, 2H), 6.96 (d, $J = 8.7$ Hz, 2H), 7.94 (d, $J = 8.7$ Hz, 2H).

1-(4-(2-(2-Hydroxyethoxy)ethoxy)ethoxy)phenyl)ethanone (8c). The reaction described above to prepare 6a was used, and 8c was obtained from 4-hydroxyacetophenone and 2-[2-(chloroethoxy)ethoxy]ethanol. ^1H NMR (CDCl_3) δ : 2.50 (s, 3H), 3.72–3.83 (m, 6H), 3.92 (t, $J = 4.5$ Hz, 2H), 4.22 (t, $J = 5.1$ Hz, 2H), 4.49 (t, $J = 4.2$ Hz, 1H), 4.61 (t, $J = 4.2$ Hz, 1H), 6.86 (d, $J = 8.7$ Hz, 2H), 7.80 (d, $J = 8.7$ Hz, 2H).

1-(4-(2-Fluoroethoxy)phenyl)ethanone (9a). The reaction described above to prepare 7a was used, and 1.02 g of 9a was obtained

in a yield of 63.3% from **8a** and DAST. $^1\text{H NMR}$ (CDCl_3) δ : 4.24 (d, t , $J_1=28.2$ Hz, $J_2=4.2$ Hz, 2H), 4.75 (d, t , $J_1=47.1$ Hz, $J_2=3.9$ Hz, 2H), 6.92 (d, $J=9.0$ Hz, 2H), 7.89 (d, $J=9.3$ Hz, 2H).

1-(4-(2-(2-Fluoroethoxy)ethoxy)phenyl)ethanone (9b). The reaction described above to prepare **7b** was used, and **9b** was obtained from **9a** and DAST. $^1\text{H NMR}$ (CDCl_3) δ : 2.56 (s, 3H), 3.78 (t, $J=3.3$ Hz, 1H), 3.86–3.94 (m, 3H), 4.22 (t, $J=5.1$ Hz, 2H), 4.51 (t, $J=3.0$ Hz, 1H), 4.67 (t, $J=3.0$ Hz, 1H), 6.96 (d, $J=8.7$ Hz, 2H), 7.93 (d, $J=8.7$ Hz, 2H). EI-MS: m/z 226 (M^+).

1-(4-(2-(2-Fluoroethoxy)ethoxy)ethoxy)phenyl)ethanone (9c). The reaction described above to prepare **7c** was used, and 543 mg of **9c** was obtained from **8c** and DAST. $^1\text{H NMR}$ (CDCl_3) δ : 2.56 (s, 3H), 3.69–3.81 (m, 6H), 3.90 (t, $J=4.5$ Hz, 2H), 4.21 (t, $J=5.1$ Hz, 2H), 4.49 (t, $J=4.2$ Hz, 1H), 4.65 (t, $J=4.2$ Hz, 1H), 6.95 (d, $J=9.3$ Hz, 2H), 7.92 (d, $J=9.0$ Hz, 2H). EI-MS: m/z 270 (M^+).

(E)-1-(4-(2-Fluoroethoxy)phenyl)-3-(4-nitrophenyl)-2-propen-1-one (10a). The reaction described above to prepare **5** was used, and 856 mg of **10a** was obtained in a yield of 56.6% from **9a** and 4-nitrobenzaldehyde. $^1\text{H NMR}$ (CDCl_3) δ : 4.32 (d, t , $J_1=27.6$ Hz, $J_2=4.2$ Hz, 2H), 4.81 (d, t , $J_1=47.4$ Hz, $J_2=4.2$ Hz, 2H), 7.04 (d, $J=8.7$ Hz, 2H), 7.65 (d, $J=15.6$ Hz, 1H), 7.79 (d, $J=8.7$ Hz, 2H), 7.82 (d, $J=12.6$ Hz, 1H), 8.06 (d, $J=9.0$ Hz, 2H), 8.28 (d, $J=8.7$ Hz, 2H).

(E)-1-(4-(2-(Fluoroethoxy)ethoxy)phenyl)-3-(4-nitrophenyl)-2-propen-1-one (10b). The reaction described above to prepare **5** was used, and 128 mg of **10b** was obtained from **9b** and 4-nitrobenzaldehyde. $^1\text{H NMR}$ (CDCl_3) δ : 3.79 (t, $J=4.2$ Hz, 1H), 3.88–4.27 (m, 3H), 4.8 (t, $J=4.8$ Hz, 2H), 4.53 (t, $J=4.2$ Hz, 1H), 4.69 (t, $J=4.2$ Hz, 1H), 7.03 (d, $J=8.7$ Hz, 2H), 7.66 (d, $J=15.6$ Hz, 1H), 7.79 (d, $J=9.0$ Hz, 2H), 7.81 (d, $J=15.6$ Hz, 1H), 8.05 (d, $J=8.7$ Hz, 2H), 8.28 (d, $J=9.0$ Hz, 2H).

(E)-1-(4-(2-(Fluoroethoxy)ethoxy)ethoxy)phenyl)-3-(4-nitrophenyl)-2-propen-1-one (10c). The reaction described above to prepare **5** was used, and 649 mg of **10c** was obtained from **9c**. $^1\text{H NMR}$ (CDCl_3) δ : 3.71–3.82 (m, 6H), 3.92 (t, $J=4.5$ Hz, 2H), 4.24 (t, $J=4.8$ Hz, 2H), 4.50 (t, $J=4.2$ Hz, 1H), 4.66 (t, $J=4.5$ Hz, 1H), 7.03 (d, $J=9.3$ Hz, 2H), 7.66 (d, $J=15.6$ Hz, 1H), 7.79 (d, $J=9.0$ Hz, 2H), 7.81 (d, $J=15.6$ Hz, 1H), 8.05 (d, $J=9.3$ Hz, 2H), 8.28 (d, $J=8.7$ Hz, 2H).

(E)-3-(4-Aminophenyl)-1-(4-(2-fluoroethoxy)phenyl)-2-propen-1-one (11a). A mixture of **10a** (856 mg, 2.7 mmol), SnCl_2 (2.55 g, 13.5 mmol), and EtOH (10 mL) was stirred at 100 °C for 2 h. After the mixture had cooled to room temperature, 1 M NaOH (10 mL) was added. The mixture was then extracted with ethyl acetate (10 mL). The organic phase was dried over Na_2SO_4 and filtered. The solvent was removed, and the residue was purified by silica gel chromatography using chloroform as a mobile phase to give 333 mg of **11a** (43.0%). $^1\text{H NMR}$ (CDCl_3) δ : 4.02 (s, broad, 2H), 4.30 (d, t , $J_1=27.6$ Hz, $J_2=4.2$ Hz, 2H), 4.79 (d, t , $J_1=47.4$ Hz, $J_2=4.2$ Hz, 2H), 6.68 (d, $J=8.7$ Hz, 2H), 7.00 (d, $J=8.7$ Hz, 2H), 7.36 (d, $J=15.3$ Hz, 1H), 7.48 (d, $J=8.4$ Hz, 2H), 7.75 (d, $J=15.3$ Hz, 1H), 8.03 (d, $J=6.9$ Hz, 2H). EI-MS: m/z 285 (M^+).

(E)-3-(4-Aminophenyl)-1-(4-(2-(fluoroethoxy)ethoxy)phenyl)-2-propen-1-one (11b). The reaction described above to prepare **11a** was used, and 85 mg of **11b** was obtained from **10b**. $^1\text{H NMR}$ (CDCl_3) δ : 3.77–3.94 (m, 4H), 4.00 (s, broad, 2H), 4.23 (t, $J=4.5$ Hz, 2H), 4.53 (t, $J=4.2$ Hz, 1H), 4.69 (t, $J=4.2$ Hz, 1H), 6.68 (d, $J=8.4$ Hz, 2H), 6.99 (d, $J=8.7$ Hz, 2H), 7.74 (d, $J=15.6$ Hz, 1H), 7.48 (d, $J=8.4$ Hz, 1H), 7.36 (d, $J=15.3$ Hz, 1H), 8.01 (d, $J=9.0$ Hz, 2H). EI-MS: m/z 329 (M^+).

(E)-3-(4-Aminophenyl)-1-(4-(2-(fluoroethoxy)ethoxy)ethoxy)phenyl)-2-propen-1-one (11c). The reaction described above to prepare **11a** was used, and 206 mg of **11c** was obtained from **10c**. $^1\text{H NMR}$ (CDCl_3) δ : 3.70–3.83 (m, 6H), 3.89 (t, $J=4.5$ Hz, 2H), 4.12 (s, broad, 2H), 4.21 (t, $J=4.8$ Hz, 2H), 4.49 (t, $J=4.0$ Hz, 1H), 4.65 (t, $J=3.9$ Hz, 1H), 6.67 (d, $J=8.7$ Hz, 2H), 6.98 (d, $J=8.7$ Hz, 2H), 7.36 (d, $J=15.3$ Hz, 1H), 7.47 (d, $J=8.4$ Hz, 2H), 7.74 (d, $J=15.9$ Hz, 1H), 8.01 (d, $J=9.0$ Hz, 2H). EI-MS: m/z 373 (M^+).

(E)-1-(4-(2-Fluoroethoxy)phenyl)-3-(4-(methylamino)phenyl)-2-propen-1-one (12a). To a solution of **11a** (290 mg, 1.02 mmol) in DMSO (6 mL) were added CH_3I (0.18 mL, 3.05 mmol) and anhydrous K_2CO_3 (691 mg, 5.08 mmol). The reaction mixture was stirred at room temperature for 3 h and poured into water. The mixture was extracted with ethyl acetate. The organic layers were combined and dried over Na_2SO_4 . Evaporation of the solvent afforded a residue, which was purified by silica gel chromatography (hexane:ethyl acetate = 2:1) to give 90 mg of **12a** (29.5%). $^1\text{H NMR}$ (CDCl_3) δ : 2.89 (s, 3H), 4.23 (d, t , $J_1=27.9$ Hz, $J_2=4.2$ Hz, 2H), 4.79 (d, t , $J_1=47.4$ Hz, $J_2=4.2$ Hz, 2H), 6.59 (d, $J=8.7$ Hz, 2H), 6.99 (d, $J=9.0$ Hz, 2H), 7.34 (d, $J=15.3$ Hz, 1H), 7.51 (d, $J=8.4$ Hz, 2H), 7.78 (d, $J=15.3$ Hz, 1H), 8.02 (d, $J=9.3$ Hz, 2H). EI-MS: m/z 299 (M^+).

(E)-1-(4-(2-(Fluoroethoxy)ethoxy)phenyl)-3-(4-(methylamino)phenyl)-2-propen-1-one (12b). The reaction described above to prepare **12a** was used, and 22 mg of **12b** was obtained from **11b**. $^1\text{H NMR}$ (CDCl_3) δ : 2.90 (s, 3H), 3.78–3.95 (m, 4H), 3.99 (s, broad, 1H), 4.23 (t, $J=4.5$ Hz, 2H), 4.53 (t, $J=4.5$ Hz, 2H), 4.53 (t, $J=4.2$ Hz, 1H), 4.69 (t, $J=4.2$ Hz, 1H), 6.60 (d, $J=8.7$ Hz, 2H), 6.99 (d, $J=8.7$ Hz, 2H), 7.35 (d, $J=15.3$ Hz, 1H), 7.51 (d, $J=8.7$ Hz, 2H), 7.77 (d, $J=15.3$ Hz, 1H), 8.02 (d, $J=8.7$ Hz, 2H). EI-MS: m/z 343 (M^+).

(E)-1-(4-(2-(Fluoroethoxy)ethoxy)ethoxy)phenyl)-3-(4-(methylamino)phenyl)-2-propen-1-one (12c). The reaction described above to prepare **12a** was used, and 53 mg of **12c** was obtained from **11c**. $^1\text{H NMR}$ (CDCl_3) δ : 2.89 (s, 3H), 3.69–3.83 (m, 6H), 3.90 (t, $J=4.8$ Hz, 2H), 4.12 (s, broad, 1H), 4.22 (t, $J=5.1$ Hz, 2H), 4.49 (t, $J=4.2$ Hz, 1H), 4.65 (t, $J=4.1$ Hz, 1H), 6.60 (d, $J=8.7$ Hz, 2H), 6.98 (d, $J=9.0$ Hz, 2H), 7.35 (d, $J=15.3$ Hz, 1H), 7.51 (d, $J=8.7$ Hz, 2H), 7.76 (d, $J=15.3$ Hz, 1H), 8.01 (d, $J=8.7$ Hz, 2H). EI-MS: m/z 387 (M^+).

(E)-3-(4-Dimethylaminophenyl)-1-(4-fluorophenyl)-2-propen-1-one (13). The reaction described above to prepare **5** was used, and 209 mg of **13** was obtained from 4-fluoroacetophenone and 4-dimethylbenzaldehyde. $^1\text{H NMR}$ (300 MHz, CDCl_3) δ : 3.03 (s, 6H), 6.68 (d, $J=8.7$ Hz, 2H), 7.15 (t, $J=8.4$ Hz, 2H), 7.30 (d, $J=15.3$ Hz, 1H), 7.54 (d, $J=9.0$ Hz, 2H), 7.78 (d, $J=15.3$ Hz, 1H), 8.02–8.06 (m, 2H). EI-MS: m/z 269 (M^+).

(E)-1-(4-Fluorophenyl)-3-(4-nitrophenyl)-2-propen-1-one (14). The reaction described above to prepare **5** was used, and 490 mg of **14** was obtained from 4-fluoroacetophenone and 4-nitrobenzaldehyde. $^1\text{H NMR}$ (300 MHz, CDCl_3) δ : 7.21 (t, $J=8.7$ Hz, 2H), 7.62 (d, $J=15.9$ Hz, 1H), 7.80 (d, $J=8.7$ Hz, 2H), 7.84 (d, $J=15.9$ Hz, 1H), 8.07–8.12 (m, 2H), 8.29 (d, $J=8.7$ Hz, 2H). EI-MS: m/z 271 (M^+).

(E)-3-(4-Aminophenyl)-1-(4-fluorophenyl)-2-propen-1-one (15). The reaction described above to prepare **11(a–c)** was used, and 150 mg of **15** was obtained from **14**. $^1\text{H NMR}$ (300 MHz, CDCl_3) δ : 4.07 (s, broad, 2H), 6.67 (d, $J=8.7$ Hz, 2H), 7.15 (t, $J=8.7$ Hz, 2H), 7.31 (d, $J=15.6$ Hz, 1H), 7.47 (d, $J=8.4$ Hz, 2H), 7.75 (d, $J=15.6$ Hz, 1H), 8.03 (t, $J=8.7$ Hz, 2H). EI-MS: m/z 241 (M^+).

(E)-1-(4-Fluorophenyl)-3-(4-methylaminophenyl)-2-propen-1-one (16). The reaction described above to prepare **12(a–c)** was used, and 14 mg of **16** was obtained from **15**. $^1\text{H NMR}$ (300 MHz, CDCl_3) δ : 2.90 (s, 3H), 4.20 (s, broad, 1H), 6.60 (d, $J=8.7$ Hz, 2H), 7.17 (d, $J=8.7$ Hz, 2H), 7.30 (d, $J=15.6$ Hz, 1H), 7.50 (d, $J=8.7$ Hz, 2H), 7.78 (d, $J=15.6$ Hz, 1H), 8.04 (d, $J=8.7$ Hz, 2H). EI-MS: m/z 255 (M^+).

(E)-2-(2-(2-(4-(3-(4-(Dimethylamino)phenyl)acryloyl)phenoxy)ethoxy)ethoxy)ethyl 4-methylbenzenesulfonate (17). To a solution of **6c** (108 mg, 0.27 mmol) in pyridine (3 mL) was added tosyl chloride (343.8 mg, 0.621 mmol). The reaction mixture was stirred for 3 h at room temperature. After water was added, the mixture was extracted with ethyl acetate. The organic layer was dried over Na_2SO_4 , and evaporation of the solvent afforded a residue, which was purified by preparative TLC (hexane:ethyl acetate = 1:1) to give 44 mg of **17** (29.4%). $^1\text{H NMR}$ (300 MHz, CDCl_3) δ : 2.43 (s, 3H), 3.04 (s, 6H), 3.62–3.72 (m, 6H),

3.85–3.87 (m, 2H), 4.15–4.18 (m, 4H), 6.70 (d, $J=8.7$ Hz, 2H), 6.98 (d, $J=9.0$ Hz, 2H), 7.31–7.35 (m, 2H), 7.37 (d, $J=9.0$ Hz, 1H), 7.55 (d, $J=8.7$ Hz, 2H), 7.80 (t, $J=8.7$ Hz, 3H), 8.02 (d, $J=9.0$ Hz, 2H). EI-MS m/z 553 (M^+)

Radiolabeling. Procedure for Labeling of 7a, 7b, 7c, and 13 with ^{11}C . ^{11}C was produced via a $^{14}\text{N}(p,\alpha)^{11}\text{C}$ reaction with 16 MeV protons on a target of nitrogen gas with an ultracompact cyclotron (CYPRIS model 325R; Sumitomo Heavy Industry Ltd.) The $^{11}\text{CO}_2$ produced was transported to an automated system for the synthesis of ^{11}C -methyl iodide (CUPID C-100; Sumitomo Heavy Industry Ltd.) and converted sequentially to $^{11}\text{C}[\text{MeOTf}]$ by the previously described method of Jewett.³³ ^{11}C Chalcones were produced by reacting $^{11}\text{C}[\text{MeOTf}]$ with the normethyl precursor, 7a, 7b, 7c, and 13, (0.5 mg) in 500 μL of methyl ethyl ketone (MEK). After the complete transfer of $^{11}\text{C}[\text{MeOTf}]$, ^{11}C -methylation was carried out for 5 min and the reaction solvent was then dried with a stream of nitrogen gas. The residue taken up in 200 μL of acetonitrile was purified by a reverse phase HPLC system (a Shimadzu LC-6A isocratic pump, a Shimadzu SPD-6A UV detector, and a Aloka NDW-351D scintillation detector) on a Cosmosil C_{18} column (Nakalai Tesque, 5C₁₈-AR-II, 10 mm \times 250 mm) with an isocratic solvent of acetonitrile/water (55/45) at a flow rate of 6.0 mL/min. The desired fraction was collected in a flask and evaporated dry. The radiochemical yield, purity, and specific activity of ^{11}C chalcones were further confirmed by analytical reverse phase HPLC on a 5C₁₈-AR-300 column (Nakalai Tesque, 4.6 mm \times 150 mm, acetonitrile/water (60/40), 1.0 mL/min).

Procedure for Labeling 7c with ^{18}F . ^{18}F Fluoride was produced by the JSW typeBC3015 cyclotron via an $^{18}\text{O}(p,n)^{18}\text{F}$ reaction and passed through a Sep-Pak Light QMA cartridge (Waters) as an aqueous solution in ^{18}O -enriched water. The cartridge was dried by airflow, and the ^{18}F activity was eluted with 0.5 mL of a Kryptofix 222/ K_2CO_3 solution (11 mg of Kryptofix 222 and 2.6 mg of K_2CO_3 in acetonitrile/water (86/14)). The solvent was removed at 120 $^\circ\text{C}$ under a stream of argon gas. The residue was azeotropically dried with 1 mL of anhydrous acetonitrile twice at 120 $^\circ\text{C}$ under a stream of nitrogen gas and dissolved in DMSO (1 mL). A solution of tosylate precursor 17 (1.0 mg) in DMSO (1 mL) was added to the reaction vessel containing the ^{18}F activity in DMSO. The mixture was heated at 160 $^\circ\text{C}$ for 5 min. Water (5 mL) was added, and the mixture was passed through a preconditioned Oasis HLB cartridge (3 cm^3) (Waters). The cartridge was washed with 10 mL of water, and the labeled compound was eluted with 2 mL of acetonitrile. The eluted compound was purified by preparative HPLC [YMC-Pack Pro C_{18} column (20 mm \times 150 mm), acetonitrile/water (75/25), flow rate 9.0 mL/min]. The retention time of the major byproduct of hydrolysis ($t_R = 2.7$ min) was well-resolved from the desired ^{18}F -labeled product ($t_R = 10.7$ min). The radiochemical purity and specific activity were determined by analytical HPLC [YMC-Pack Pro C_{18} column (4.6 mm \times 150 mm), acetonitrile/water (60/40), flow rate 1.0 mL/min], and ^{18}F 7c was obtained in a radiochemical purity of >99% with the specific activity of 35 GBq/mmol. Specific activity was estimated by comparing the UV peak intensity of the purified ^{18}F -labeled compound with a reference nonradioactive compound of known concentration.

Binding Assays Using the Aggregated A β peptides in Solution. A β (1–42) was purchased from Peptide Institute (Osaka, Japan). Aggregation was carried out by gently dissolving the peptide (0.25 mg/mL) in a buffer solution (pH 7.4) containing 10 mM sodium phosphate and 1 mM EDTA. The solution was incubated at 37 $^\circ\text{C}$ for 42 h with gentle and constant shaking. Binding experiments were carried out as described previously.¹⁸ ^{125}I DMIC with 2200 Ci/mmol of specific activity and radiochemical purity greater than 95% was prepared using the standard iododestannylation reaction. A mixture

containing 50 μL of test compound (0.2 pM–400 μM in 10% EtOH), 50 μL of 0.02 nM [^{125}I]DMIC, 50 μL of A β (1–42) aggregates, and 850 μL of 10% EtOH was incubated at room temperature for 3 h. The mixture was then filtered through Whatman GF/B filters using a Brandel M-24 cell harvester, and the radioactivity of the filters containing the bound ^{125}I ligand was measured in a γ counter. Values for the half-maximal inhibitory concentration (IC_{50}) were determined from displacement curves of three independent experiments using GraphPad Prism 4.0, and those for the inhibition constant (K_i) were calculated using the Cheng–Prusoff equation: $K_i = \text{IC}_{50}/(1 + [\text{L}]/K_d)$, where [L] is the concentration of [^{125}I]DMIC used in the assay and K_d is the dissociation constant of DMIC (4.2 nM).¹⁹ DMIC and IMPY used as test compounds for the inhibition assay were synthesized as reported previously.^{19,34}

Biodistribution in Normal Mice. Experiments with animals were conducted in accordance with our institutional guidelines and approved by the Nagasaki University Animal Care Committee and the Kyoto University Animal Care Committee. A 100 μL amount of a saline solution containing the radiolabeled agent (3.7 MBq), EtOH (10%), and ascorbic acid (1 mg/mL) was injected directly into the tail vein of ddY mice (5-week-old, 22–25 g). Groups of five mice were sacrificed at various post-injection time points. The organs of interest were removed and weighed, and the radioactivity was measured with an automatic γ counter (COBRAII, Packard).

Staining of A β Plaques in Brain Sections of Tg2576 Transgenic Mice. The Tg2576 transgenic mice (female, 20-month-old) and wild-type (female, 20-month-old) mice were used as an Alzheimer's model and an age-matched control, respectively. After the mice were sacrificed by decapitation, the brains were immediately removed and frozen in powdered dry ice. The frozen blocks were sliced into serial sections 10 μm thick. Each slide was incubated with a 50% EtOH solution (100 μM) of compound 7c for 10 min. The sections were washed with 50% EtOH for 3 min two times. After drying, the sections were then examined using a microscope (Nikon, Eclipse 80i) equipped with a B-2A filter set (excitation, 450–490 nm; dichroic mirror, 505 nm; long-pass filter, 520 nm). Thereafter, the serial sections were also immunostained with 3,3'-diaminobenzidine (DAB) as a chromogen using monoclonal antibodies against A β (amyloid β -protein immunohistostain kit, WAKO).

In Vitro Autoradiography Using Human AD Brains. Postmortem brain tissues from an autopsy-confirmed case of AD (73-year-old male) were obtained from BioChain Institute Inc. The presence and localization of plaques on the sections were confirmed with immunohistochemical staining using a monoclonal A β antibody as described above. The sections were incubated with [^{18}F]7c (54 $\mu\text{Ci}/200 \mu\text{L}$) for 1 h at room temperature. They were then washed in 50% EtOH (two 1 min wash), before being rinsed with water for 30 s. After drying, the ^{18}F -labeled sections were exposed to a BAS imaging plate (Fuji Film, Tokyo, Japan) for 6 h. Ex vivo autoradiographic images were obtained using a BAS5000 scanner system (Fuji Film). After autoradiographic examination, the same sections were stained by thioflavin-S to confirm the presence of A β plaques. For the staining of thioflavin-S, sections were immersed in a 0.125% thioflavin-S solution containing 50% EtOH for 3 min and washed in 50% EtOH. After drying, the sections were then examined using a microscope (Nikon, Eclipse 80i) equipped with a B-2A filter set (excitation, 450–490 nm; dichroic mirror, 505 nm; long-pass filter, 520 nm).

Acknowledgment. This study was supported by the Program for Promotion of Fundamental Studies in Health Sciences of the National Institute of Biomedical Innovation (NIBIO), a Health Labour Sciences Research Grant, and a Grant-in-Aid for Young Scientists (A) and Exploratory Research from the Ministry of Education, Culture, Sports, Science and Technology, Japan.

Supporting Information Available: Representative HPLC chromatograms of [¹⁸F]7c. This material is available free of charge via the Internet at <http://pubs.acs.org>.

References

- (1) Hardy, J. A.; Higgins, G. A. Alzheimer's disease: the amyloid cascade hypothesis. *Science* **1992**, *256*, 184–185.
- (2) Selkoe, D. J. Alzheimer's disease: genes, proteins, and therapy. *Physiol. Rev.* **2001**, *81*, 741–766.
- (3) Nordberg, A. PET imaging of amyloid in Alzheimer's disease. *Lancet Neurol.* **2004**, *3*, 519–527.
- (4) Mathis, C. A.; Wang, Y.; Klunk, W. E. Imaging β -amyloid plaques and neurofibrillary tangles in the aging human brain. *Curr. Pharm. Des.* **2004**, *10*, 1469–1492.
- (5) Klunk, W. E.; Engler, H.; Nordberg, A.; Wang, Y.; Blomqvist, G.; Holt, D. P.; Bergstrom, M.; Savitcheva, I.; Huang, G. F.; Estrada, S.; Ausen, B.; Debnath, M. L.; Barletta, J.; Price, J. C.; Sandell, J.; Lopresti, B. J.; Wall, A.; Koivisto, P.; Antoni, G.; Mathis, C. A.; Langstrom, B. Imaging brain amyloid in Alzheimer's disease with Pittsburgh Compound-B. *Ann. Neurol.* **2004**, *55*, 306–319.
- (6) Mathis, C. A.; Wang, Y.; Holt, D. P.; Huang, G. F.; Debnath, M. L.; Klunk, W. E. Synthesis and evaluation of ¹¹C-labeled 6-substituted 2-arylbenzothiazoles as amyloid imaging agents. *J. Med. Chem.* **2003**, *46*, 2740–2754.
- (7) Verhoeff, N. P.; Wilson, A. A.; Takeshita, S.; Trop, L.; Hussey, D.; Singh, K.; Kung, H. F.; Kung, M. P.; Houle, S. In vivo imaging of Alzheimer disease β -amyloid with [¹¹C]SB-13 PET. *Am. J. Geriatr. Psychiatry* **2004**, *12*, 584–595.
- (8) Ono, M.; Wilson, A.; Nobrega, J.; Westaway, D.; Verhoeff, P.; Zhuang, Z. P.; Kung, M. P.; Kung, H. F. ¹¹C-Labeled stilbene derivatives as A β -aggregate-specific PET imaging agents for Alzheimer's disease. *Nucl. Med. Biol.* **2003**, *30*, 565–571.
- (9) Small, G. W.; Kepe, V.; Ercoli, L. M.; Siddarth, P.; Bookheimer, S. Y.; Miller, K. J.; Lavretsky, H.; Burggren, A. C.; Cole, G. M.; Vinters, H. V.; Thompson, P. M.; Huang, S. C.; Satyamurthy, N.; Phelps, M. E.; Barrio, J. R. PET of brain amyloid and tau in mild cognitive impairment. *N. Engl. J. Med.* **2006**, *355*, 2652–2663.
- (10) Shoghi-Jadid, K.; Small, G. W.; Agdeppa, E. D.; Kepe, V.; Ercoli, L. M.; Siddarth, P.; Read, S.; Satyamurthy, N.; Petric, A.; Huang, S. C.; Barrio, J. R. Localization of neurofibrillary tangles and β -amyloid plaques in the brains of living patients with Alzheimer disease. *Am. J. Geriatr. Psychiatry* **2002**, *10*, 24–35.
- (11) Rowe, C. C.; Ackerman, U.; Browne, W.; Mulligan, R.; Pike, K. L.; O'Keefe, G.; Tochon-Danguy, H.; Chan, G.; Berlangieri, S. U.; Jones, G.; Dickinson-Rowe, K. L.; Kung, H. P.; Zhang, W.; Kung, M. P.; Skovronsky, D.; Dyrks, T.; Holl, G.; Krause, S.; Friebe, M.; Lehman, L.; Lindemann, S.; Dinkelborg, L. M.; Masters, C. L.; Villemagne, V. L. Imaging of amyloid β in Alzheimer's disease with ¹⁸F-BAY94-9172, a novel PET tracer: proof of mechanism. *Lancet Neurol.* **2008**, *7*, 129–135.
- (12) Zhang, W.; Oya, S.; Kung, M. P.; Hou, C.; Maier, D. L.; Kung, H. F. F-18 polyethyleneglycol stilbenes as PET imaging agents targeting A β aggregates in the brain. *Nucl. Med. Biol.* **2005**, *32*, 799–809.
- (13) Lockhart, A. Imaging Alzheimer's disease pathology: one target, many ligands. *Drug Discovery Today* **2006**, *11*, 1093–1099.
- (14) Ye, L.; Morgenstern, J. L.; Gee, A. D.; Hong, G.; Brown, J.; Lockhart, A. Delineation of positron emission tomography imaging agent binding sites on β -amyloid peptide fibrils. *J. Biol. Chem.* **2005**, *280*, 23599–235604.
- (15) Lockhart, A.; Ye, L.; Judd, D. B.; Merritt, A. T.; Lowe, P. N.; Morgenstern, J. L.; Hong, G.; Gee, A. D.; Brown, J. Evidence for the presence of three distinct binding sites for the thioflavin T class of Alzheimer's disease PET imaging agents on β -amyloid peptide fibrils. *J. Biol. Chem.* **2005**, *280*, 7677–7684.
- (16) Ono, M.; Yoshida, N.; Ishibashi, K.; Haratake, M.; Arano, Y.; Mori, H.; Nakayama, M. Radioiodinated flavones for in vivo imaging of β -amyloid plaques in the brain. *J. Med. Chem.* **2005**, *48*, 7253–7260.
- (17) Ono, M.; Watanabe, R.; Kawashima, H.; Kawai, T.; Watanabe, H.; Haratake, M.; Saji, H.; Nakayama, M. ¹⁸F-Labeled flavones for in vivo imaging of β -amyloid plaques in Alzheimer's brains. *Bioorg. Med. Chem.* **2009**, *17*, 2069–2076.
- (18) Ono, M.; Hori, M.; Haratake, M.; Tomiyama, T.; Mori, H.; Nakayama, M. Structure–activity relationship of chalcones and related derivatives as ligands for detecting of β -amyloid plaques in the brain. *Bioorg. Med. Chem.* **2007**, *15*, 6388–6396.
- (19) Ono, M.; Haratake, M.; Mori, H.; Nakayama, M. Novel chalcones as probes for in vivo imaging of β -amyloid plaques in Alzheimer's brains. *Bioorg. Med. Chem.* **2007**, *15*, 6802–6809.
- (20) Maya, Y.; Ono, M.; Watanabe, H.; Haratake, M.; Saji, H.; Nakayama, M. Novel radioiodinated aurones as probes for SPECT imaging of β -amyloid plaques in the brain. *Bioconjugate Chem.* **2009**, *20*, 95–101.
- (21) Ono, M.; Maya, Y.; Haratake, M.; Ito, K.; Mori, H.; Nakayama, M. Aurones serve as probes of β -amyloid plaques in Alzheimer's disease. *Biochem. Biophys. Res. Commun.* **2007**, *361*, 116–121.
- (22) Stephenson, K. A.; Chandra, R.; Zhuang, Z. P.; Hou, C.; Oya, S.; Kung, M. P.; Kung, H. F. Fluoro-pegylated (FPEG) imaging agents targeting A β aggregates. *Bioconjugate Chem.* **2007**, *18*, 238–246.
- (23) Qu, W.; Kung, M. P.; Hou, C.; Oya, S.; Kung, H. F. Quick assembly of 1,4-diphenyltriazoles as probes targeting β -amyloid aggregates in Alzheimer's disease. *J. Med. Chem.* **2007**, *50*, 3380–3387.
- (24) Zhang, W.; Oya, S.; Kung, M. P.; Hou, C.; Maier, D. L.; Kung, H. F. F-18 stilbenes as PET imaging agents for detecting β -amyloid plaques in the brain. *J. Med. Chem.* **2005**, *48*, 5980–5988.
- (25) Kung, M. P.; Hou, C.; Zhuang, Z. P.; Zhang, B.; Skovronsky, D.; Trojanowski, J. Q.; Lee, V. M.; Kung, H. F. IMPY: an improved thioflavin-T derivative for in vivo labeling of β -amyloid plaques. *Brain Res.* **2002**, *956*, 202–210.
- (26) Hsiao, K.; Chapman, P.; Nilsen, S.; Eckman, C.; Harigaya, Y.; Younkin, S.; Yang, F.; Cole, G. Correlative memory deficits, A β elevation, and amyloid plaques in transgenic mice. *Science* **1996**, *274*, 99–102.
- (27) Kuntner, C.; Kesner, A. L.; Bauer, M.; Kramslehner, R.; Wanek, T.; Mandler, M.; Karch, R.; Stanek, J.; Wolf, T.; Muller, M.; Langer, O. Limitations of small animal PET imaging with [¹⁸F]FDDNP and FDG for quantitative studies in a transgenic mouse model of Alzheimer's disease. *Mol. Imaging Biol.* **2009**, *11*, 236–240.
- (28) Klunk, W. E.; Lopresti, B. J.; Ikonovic, M. D.; Lefterov, I. M.; Koldamova, R. P.; Abrahamson, E. E.; Debnath, M. L.; Holt, D. P.; Huang, G. F.; Shao, L.; DeKosky, S. T.; Price, J. C.; Mathis, C. A. Binding of the positron emission tomography tracer Pittsburgh compound-B reflects the amount of amyloid- β in Alzheimer's disease brain but not in transgenic mouse brain. *J. Neurosci.* **2005**, *25*, 10598–10606.
- (29) Maeda, J.; Ji, B.; Irie, T.; Tomiyama, T.; Maruyama, M.; Okauchi, T.; Staufenbiel, M.; Iwata, N.; Ono, M.; Saido, T. C.; Suzuki, K.; Mori, H.; Higuchi, M.; Suhara, T. Longitudinal, quantitative assessment of amyloid, neuroinflammation, and anti-amyloid treatment in a living mouse model of Alzheimer's disease enabled by positron emission tomography. *J. Neurosci.* **2007**, *27*, 10957–10968.
- (30) Toyama, H.; Ye, D.; Ichise, M.; Liow, J. S.; Cai, L.; Jacobowitz, D.; Musachio, J. L.; Hong, J.; Crescenzo, M.; Tipre, D.; Lu, J. Q.; Zoghbi, S.; Vines, D. C.; Seidel, J.; Katada, K.; Green, M. V.; Pike, V. W.; Cohen, R. M.; Innis, R. B. PET imaging of brain with the β -amyloid probe, [¹¹C]6-OH-BTA-1, in a transgenic mouse model of Alzheimer's disease. *Eur. J. Nucl. Med. Mol. Imaging* **2005**, *32*, 593–600.
- (31) Skovronsky, D. M.; Zhang, B.; Kung, M. P.; Kung, H. F.; Trojanowski, J. Q.; Lee, V. M. In vivo detection of amyloid plaques in a mouse model of Alzheimer's disease. *Proc. Natl. Acad. Sci. U.S.A.* **2000**, *97*, 7609–7614.
- (32) Saido, T. C.; Iwatsubo, T.; Mann, D. M.; Shimada, H.; Ihara, Y.; Kawashima, S. Dominant and differential deposition of distinct β -amyloid peptide species, A β N3(pE), in senile plaques. *Neuron* **1995**, *14*, 457–466.
- (33) Jewett, D. M. A simple synthesis of [¹¹C]methyl triflate. *Int. J. Radiat. Appl. Instrum. A* **1992**, *43*, 1383–1385.
- (34) Zhuang, Z. P.; Kung, M. P.; Wilson, A.; Lee, C. W.; Plossl, K.; Hou, C.; Holtzman, D. M.; Kung, H. F. Structure–activity relationship of imidazo[1,2-a]pyridines as ligands for detecting β -amyloid plaques in the brain. *J. Med. Chem.* **2003**, *46*, 237–243.



Synthesis and evaluation of a radioiodinated lumiracoxib derivative for the imaging of cyclooxygenase-2 expression

Yuji Kuge^{a,b,*}, Naoyuki Obokata^a, Hiroyuki Kimura^a, Yumiko Katada^a, Takashi Temma^a, Yukihiko Sugimoto^c, Kazuki Aita^{a,d}, Koh-ichi Seki^d, Nagara Tamaki^e, Hideo Saji^a

^aDepartment of Patho-Functional Bioanalysis, Graduate School of Pharmaceutical Sciences, Kyoto University, Kyoto 606-8501, Japan

^bDepartment of Tracer Kinetics and Bioanalysis, Graduate School of Medicine, Hokkaido University, Sapporo 060-8638, Japan

^cDepartment of Physiological Chemistry, Graduate School of Pharmaceutical Sciences, Kyoto University, Kyoto 606-8501, Japan

^dCentral Institute of Isotope Science, Hokkaido University, Sapporo 060-8638, Japan

^eDepartment of Nuclear Medicine, Graduate School of Medicine, Hokkaido University, Sapporo 060-8638, Japan

Received 18 February 2009; received in revised form 14 July 2009; accepted 26 July 2009

Abstract

Introduction: Despite extensive attempts to develop cyclooxygenase (COX)-2 imaging radiotracers, no suitable positron emission tomography (PET)/single photon emission computed tomography (SPECT) tracers are currently available for in vivo imaging of COX-2 expression. The aims of this study were to synthesize and evaluate a radioiodinated derivative of lumiracoxib, 2-[(2-fluoro-6-iodophenyl)-amino]-5-methylphenylacetic acid (FIMA), which is structurally distinct from other drugs in the class and has weakly acidic properties, as a SPECT tracer for imaging COX-2 expression.

Methods: The COX inhibitory potency was assessed by measuring COX-catalyzed oxidation with hydrogen peroxide. Cell uptake characteristics of ¹²⁵I-FIMA were assessed in control and interferon- γ -stimulated macrophages. The biodistribution of ¹²⁵I-FIMA was determined by the ex vivo tissue counting method in rats.

Results: The COX-2 inhibitory potency of FIMA ($IC_{50}=2.46 \mu M$) was higher than that of indomethacin ($IC_{50}=20.9 \mu M$) and was comparable to lumiracoxib ($IC_{50}=0.77 \mu M$) and diclofenac ($IC_{50}=0.98 \mu M$). The IC_{50} ratio (COX-1/COX-2=182) indicated FIMA has a high isoform selectivity for COX-2. ¹²⁵I-FIMA showed a significantly higher accumulation in COX-2 induced macrophages than in control macrophages, which decreased with nonradioactive FIMA in a concentration dependent manner. The biodistribution study showed rapid clearance of ¹²⁵I-FIMA from the blood and most organs including the liver and kidneys. No significant in vivo deiodination was observed with radioiodinated FIMA.

Conclusions: FIMA showed high inhibitory potency and selectivity for COX-2. Radioiodinated FIMA showed specific accumulation into COX-2 induced macrophages, no significant in vivo deiodination and rapid blood clearance. Radioiodinated FIMA deserves further investigation as a SPECT radiopharmaceutical for imaging COX-2 expression.

© 2009 Elsevier Inc. All rights reserved.

Keywords: Cyclooxygenase-2; Inhibitor; Radioiodination; SPECT; Radiopharmaceutical

1. Introduction

Cyclooxygenases (COXs) are the key rate-limiting enzymes in the conversion of arachidonic acid to pros-

taglandins and thromboxanes. To date, at least two distinct isoforms of the COXs, a constitutive isoform (COX-1) and an inducible isoform (COX-2), and several of their variants have been discovered [1]. COX-2 plays important roles in response to inflammatory stimuli and has been implicated in a number of pathological processes including many human cancers, atherosclerosis and cerebral and cardiac ischemia [2–5]. We have also reported the association of COX-2 expression with cerebral ischemia and

* Corresponding author. Department of Tracer Kinetics and Bioanalysis, Graduate School of Medicine, Hokkaido University, Sapporo 060-8638, Japan. Tel.: +81 11 706 5085, fax: +81 11 706 7155.

E-mail address: kuge@med.hokudai.ac.jp (Y. Kuge).

atherosclerosis using rodent and primate models of these diseases [6–11].

Accordingly, noninvasive imaging of COX-2 expression would be useful for early diagnosis and for monitoring the progression and treatment efficacy for such diseases [12,13]. In this regard, several COX-2 inhibitors including ^{18}F -SC58125, ^{18}F -desbromo-DuP-697, ^{11}C -celecoxib, ^{11}C -rofecoxib and ^{123}I -celecoxib analogues have been radiolabeled and evaluated as potential tracers for positron emission tomography (PET) and single photon emission tomography (SPECT) [14–24] (Fig. 1). We have contributed to this area with the synthesis and preliminary evaluation of radioiodinated celecoxib analogues [22]. Results, however, have not been entirely consistent between laboratories due to what is generally ascribed to the relatively high nonspecific binding of these compounds [23–26]. The effect of this high nonspecific binding on results appears to be largely dependent on experimental conditions and could cause inconsistent findings. Thus, no appropriate PET/SPECT tracers are currently available for in vivo imaging of COX-2 expression [23–25]. In the search for suitable PET/SPECT tracers for COX-2 imaging, attempts have recently been made to radiolabel new generation COX-2 inhibitors which have greater inhibitory potencies and selectivities for COX-2 [25–27]. However, to date, the radiolabeled COX-2 inhibitors evaluated as PET/SPECT tracers exclusively possess the same basic skeleton, a cyclic core with two vicinal aryl rings.

Another new generation COX-2 selective inhibitor, lumiracoxib, is structurally distinct from other drugs in the class and has weakly acidic properties [28–31]. The K_i and IC_{50} values of lumiracoxib for COX-2 are better than or comparable to those of other COX-2 inhibitors including celecoxib [28]. Lumiracoxib is distributed and retained in inflamed tissues while being rapidly cleared from plasma

with a short elimination half-life [30–32]. Thus, we selected lumiracoxib as a lead compound for a potential COX-2 imaging tracer. In this study, a radioiodinated derivative of lumiracoxib, 2-[(2-Fluoro-6-iodophenyl)-amino]-5-methylphenylacetic acid (FIMA) was synthesized and its potential as an imaging tracer was assessed in both in vitro and in vivo experiments.

2. Materials and methods

2.1. General

Sodium ^{125}I -iodide (642.8 GBq/mg) was purchased from Perkin Elmer Life and Analytical Sciences (Boston, MA, USA). All chemicals used were of reagent grade.

Proton and carbon nuclear magnetic resonance spectra were recorded on a JMM-ECA500KP spectrometer (JEOL, Tokyo, Japan). The chemical shifts are reported in parts per million (ppm) downfield from an internal tetramethylsilane standard. Mass spectra were recorded with a JMS-HX/HX110A, JMS-SX102AQQ or JMS-GC-mate spectrometer (JEOL).

2.2. Synthesis

2.2.1. Synthesis of FIMA (5)

FIMA was synthesized according to the procedure outlined in Fig. 2.

Compound **2** was synthesized in three steps according to the method reported by Acemoglu et al. [33]. Briefly, *p*-iodotoluene (189 μl , 1.4 mmol) was coupled with 2-bromo-6-fluoroaniline (158 μl , 1.4 mmol), utilizing the Pd(0) catalyzed Buchwald–Hartwig reaction, to give **1** as a colorless oil with a yield of 27%. Compound **1** (771.5 mg, 2.75 mmol) was acylated with bromoacetyl bromide (288 μl , 3.30 mmol) and then subjected to a Friedel-Crafts alkylation to obtain **2** as a yellowish powder with a yield of 39% (Mp, 118–120°C).

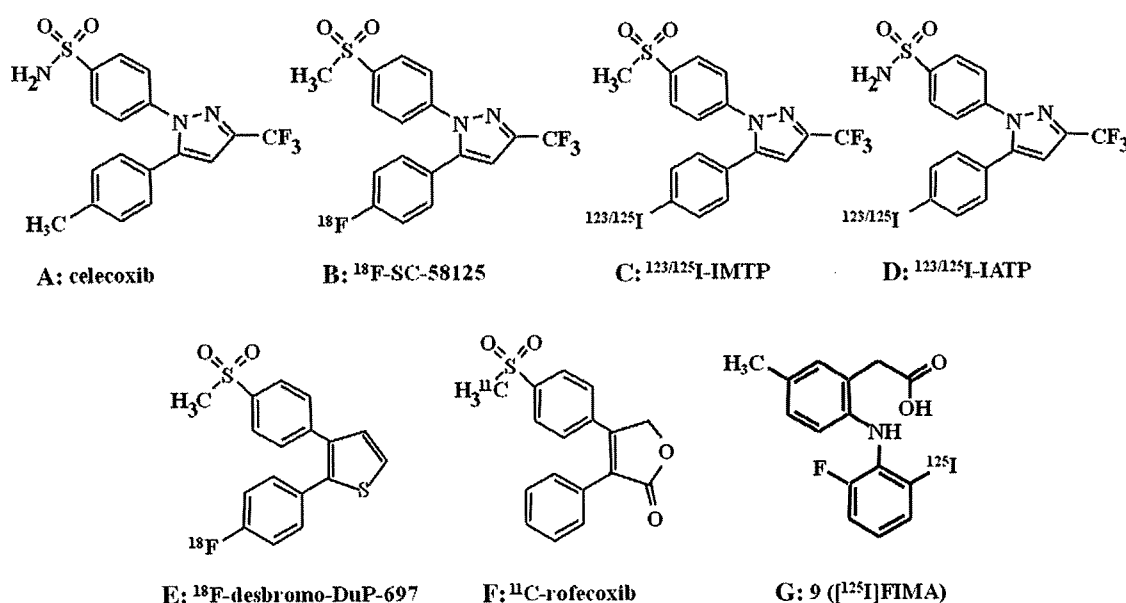


Fig. 1. Chemical structures of radiolabeled COX-2 inhibitors.

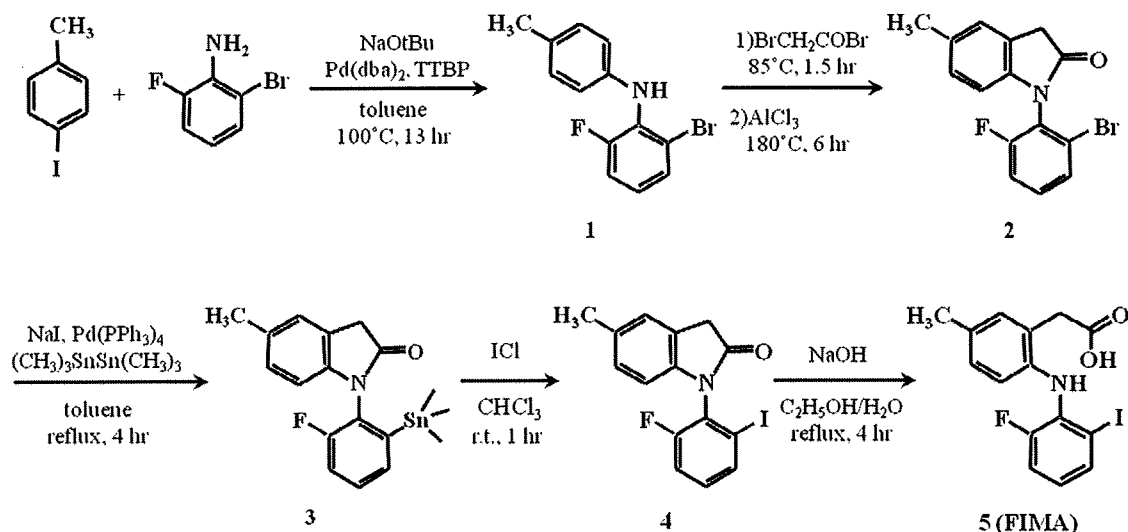


Fig. 2. Synthesis of FIMA (compound 5). Compound 1, *N*-(2-Bromo-6-fluorophenyl)-4-methylaniline; Compound 2, *N*-(2'-Bromo-6'-fluorophenyl)-5-methyloxindole; Compound 3, *N*-(2'-fluoro-6'-trimethylstannanylphenyl)-5-methyl-oxindole; Compound 4, *N*-(2'-Fluoro-6'-iodophenyl)-5-methyloxindole; Compound 5, FIMA.

To a solution of 2 (140.7 mg, 0.44 mmol) in 10 ml of toluene at room temperature under a nitrogen atmosphere, NaI (197.6 mg, 1.32 mmol) was added. After stirring at 85°C for 30 min, tetrakis(triphenylphosphine)-palladium(0) (127 mg, 0.11 mmol) and hexamethylditin(IV) (182.3 μl, 0.88 mmol) were added and the solution was refluxed for 4 h. The reaction mixture was filtered and evaporated in vacuo. The residue was purified by silica gel column chromatography (*n*-hexane/ethyl acetate, 6/1) to give 3 as a yellowish powder with a yield of 38% (Mp, 124–127°C).

To a solution of 3 (96.9 mg, 0.24 mmol) in 1 ml of chloroform under an argon atmosphere, iodine monochloride (46.7 mg, 0.29 mmol) in 1 ml of chloroform was added, and

the mixture was stirred at room temperature for 1 h. The reaction mixture was washed with saturated sodium thiosulfate and extracted with chloroform. The organic layer was dried over Na₂SO₄, filtered and concentrated in vacuo. The residue was purified by silica gel column chromatography (*n*-hexane/ethyl acetate, 4/1) to give 4 as a pinkish powder with a yield of 85% (Mp, 149–153°C).

To a solution of 4 (61.4 mg, 0.17 mmol) in EtOH/purified water (750 μl/60 μl) under reflux at 95°C, 30% (w/w) NaOH (60 μl) was added dropwise, and the reaction was further refluxed for 4 h. The reaction mixture was allowed to cool to room temperature and then was acidified with 12 N HCl to pH 3.0. Purified water was added to the mixture to give a

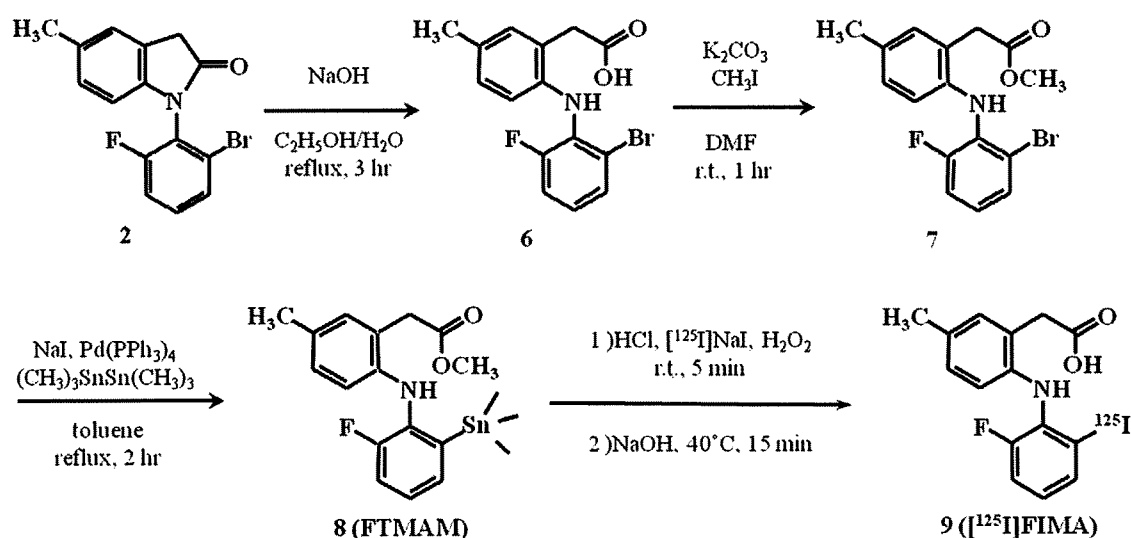


Fig. 3. Synthesis of FTMAM (Compound 8) and ¹²⁵I-FIMA (compound 9). Compound 2, *N*-(2'-Bromo-6'-fluorophenyl)-5-methyloxindole; Compound 6, 2-[(2-bromo-6-fluorophenyl)amino]-5-methylphenylacetic acid; Compound 7, 2-[(2-bromo-6-fluorophenyl)amino]-5-methylphenylacetic acid methyl ester; Compound 8, FTMAM; Compound 9, 2-[(2-fluoro-6-[¹²⁵I]iodophenyl)amino]-5-methylphenylacetic acid (¹²⁵I-FIMA).

precipitate. The precipitate was filtered, washed with purified water and dried to give **5** as a yellowish ocher powder with a yield of 92% (Mp, 149–152°C). ¹H NMR (500 MHz, CDCl₃) δ, 7.60 (dt, *J*=8.0, 1.2 Hz, 1H), 7.03–7.07 (m, 2H), 6.96 (dd, *J*=8.0, 1.6 Hz, 1H), 6.74 (td, *J*=8.1, 5.2 Hz, 1H), 6.59 (dd, *J*=8.2, 2.4 Hz, 1H), 6.30 (br s, 1H), 3.79 (s, 2H), 2.28 (s, 3H). HRFABMS: Calcd for C₁₅H₁₃FINO₂ (M+H)⁺, *m/z* 384.9975, found 384.9971.

2.2.2. Synthesis of 2-[(2-fluoro-6-trimethylstannanylphenyl)amino]-5-methylphenylacetic acid methyl ester (**8**)

2-[(2-Fluoro-6-trimethylstannanylphenyl)amino]-5-methylphenylacetic acid methyl ester (FTMAM) was synthesized according to the procedure outlined in Fig. 3. Compound **6** was synthesized from **2** with a yield of 98% (Mp, 131–134°C) using the same procedure as for FIMA from **4**. To a solution of **6** (142 mg, 0.42 mmol) in 4 ml of Dimethylformamide at room temperature under a nitrogen atmosphere, K₂CO₃ (87.1 mg, 0.63 mmol) was added, and the mixture was stirred for 10 min. Methyl iodide (39.3 μl, 0.63 mmol) was added to the reaction mixture, and the mixture was further stirred at room temperature for 1 h. After the completion of the reaction, ice chilled, purified water was added and the mixture was extracted with ethyl acetate. The organic layer was dried over Na₂SO₄, filtered and concentrated in vacuo. The crude product was purified by silica gel column chromatography (*n*-hexane/ethyl acetate, 4/1) to give **7** as a colorless solid with a yield of 95% (Mp, 55–60°C). FTMAM (**8**) was synthesized from **7** in a similar procedure as for **3** from **2**, except that the crude product was purified by preparative TLC (*n*-hexane/ethyl acetate, 4/1) to give FTMAM (**8**) as a colorless oil with a yield of 30%. Compound **6**: ¹H NMR (400 MHz, DMSO-*d*₆) δ, 7.50 (dt, *J*=8.2, 1.2 Hz, 1H), 7.27 (ddd, *J*=10.9, 8.3, 1.2 Hz, 1H), 7.01–7.07 (m, 3H), 6.90 (dd, *J*=8.0, 1.2 Hz, 1H), 6.39 (dd, *J*=8.0, 2.6 Hz, 1H), 3.63 (s, 2H), 2.21 (s, 3H). HREIMS: Calcd for C₁₅H₁₃BrFNO₂ (M+H)⁺, *m/z* 337.0113, found 337.0120. Compound **7**: ¹H NMR (500 MHz, CDCl₃) δ, 7.37 (d, *J*=8.2 Hz, 1H), 7.01–7.04 (m, 2H), 6.95 (d, *J*=8.0 Hz, 1H), 6.85 (ddd, *J*=8.2, 8.0, 5.4 Hz, 1H), 6.63–6.65 (m, 2H), 3.76 (s, 2H), 3.74 (s, 3H), 2.28 (s, 3H). HREIMS: Calcd for C₁₆H₁₅BrFNO₂ (M+H)⁺, *m/z* 351.0270, found 351.0264. Compound **8** (FTMAM): ¹H NMR (500 MHz, acetone-*d*₆) δ, 7.32 (dd, *J*=7.2, 1.4 Hz, 1H), 7.25 (ddd, *J*=8.1, 7.2, 4.5 Hz, 1H), 7.17 (ddd, *J*=10.6, 8.1, 1.4 Hz, 1H), 7.02 (s, 1H), 6.86 (d, *J*=8.2 Hz, 1H), 6.59 (br s, 1H), 6.28 (d, *J*=8.2 Hz, 1H), 3.76 (s, 2H), 3.70 (s, 3H), 2.21 (s, 3H), 0.11 (s, 9H). HREIMS: Calcd for C₁₉H₂₄FNO₂Sn (M+H)⁺, *m/z* 437.0813, found 437.0808.

2.2.3. Synthesis of lumiracoxib

Lumiracoxib, synthesized according to the method of Acemoglu et al. [33] using *p*-iodotoluene and 2-chloro-6-fluoroaniline as starting materials, was obtained as a brownish powder. ¹H NMR (400 MHz, DMSO-*d*₆) δ, 12.65 (br s, 1H), 7.35 (dd, *J*=8.3, 1.2 Hz, 1H), 7.23 (ddd,

J=9.5, 8.3, 1.2 Hz, 1H), 7.06–7.11 (m, 2H), 7.01 (br s, 1H), 6.91 (br d, *J*=8.0 Hz, 1H), 6.42 (dd, *J*=8.3, 2.9 Hz, 1H), 3.65 (s, 2H), 2.21 (s, 3H). HRFABMS: Calcd for C₁₅H₁₃ClFNO₂ (M+H)⁺, *m/z* 293.0619, found 293.0622.

2.3. Radiolabeling

Electrophilic iododestannylation of FTMAM (**8**) with sodium ¹²⁵I-iodine and H₂O₂ generated ¹²⁵I-FIMA as outlined in Fig. 3. Briefly, to a solution of FTMAM in 10 μl of EtOH (1 mg/ml) in a vial, 1 N HCl (15 μl), 12.3 MBq of sodium ¹²⁵I-iodine in 0.2 N NaOH (7.5 μl, carrier-free) and 30% H₂O₂ (2 μl) were added, and the mixture was stirred at room temperature for 5 min. After cooling with ice, saturated NaHSO₃ was added to the reaction mixture to terminate the reaction. The reaction mixture was basified with 1 N NaOH to pH 9.0 at room temperature and then was stirred at 40 °C for 15 min. The solution was applied to a reverse-phase high-performance liquid chromatography (HPLC) column (Cosmosil 5C18-AR-II 4.6 mm injected does × 150 mm, Nacalai Tesque, Kyoto, Japan) and eluted at a flow rate of 1.0 ml/min with 20 mM phosphate buffer (pH 2.5): MeOH=30: 70 for the purification of ¹²⁵I-FIMA (*R*_t=17 min). The radiochemical purity of the labeled compound was determined by analytical HPLC using the same conditions as described above. The radiochemical purity and specific activity were determined to be greater than 95% (*n*=3) and 47–72 GBq/μmol (*n*=3), respectively.

2.4. COX inhibitory potency

Peroxidase inhibitory activity of FIMA was assessed by measuring the COX-catalyzed oxidation of *N,N,N',N'*-tetramethyl-*p*-phenylenediamine (TMPD) by hydrogen peroxide using a commercially available kit (Colorimetric COX Inhibitor Screening Assay Kit, Cayman Chemical, Ann Arbor, MI, USA) as previously described [22]. Briefly, 10 μl of ovine COX-1 or COX-2 solution was added to a 96-well plate with 150 μl of 0.1 mol/L Tris buffer at pH 8.0, 10 μl of heme solution in DMSO, and 10 μl of the test compound (final concentration: 10⁻³–10⁻⁹ mol/L). After a 5-min incubation at 25°C, 20 μl of TMPD and 20 μl of 1.1 mM arachidonic acid were added to the mixture. The oxidation of TMPD was monitored by measuring the absorbance of the mixture with a plate reader at 600 nm. Lumiracoxib, diclofenac and indomethacin were used as reference compounds.

2.5. Distribution coefficients

¹²⁵I-FIMA in a mixture of 2 ml of octanol and 2 ml of 0.1 M phosphate buffer (pH 7.4) was shaken three times for 1 min and then left for 20 min. This procedure was repeated three times, and then the layers were separated by centrifugation. An aliquot of each layer was counted in an auto well gamma counter (Cobra II Auto-Gamma, Packard, Tokyo, Japan). The mean of 3–4 independent octanol-buffer distribution coefficient measurements was expressed as the

$\log D_{7.4}$. Radioiodinated analogues of celecoxib, 5-(4-[^{125}I]iodophenyl)-1-[4-(methylsulfonyl)phenyl]-3-trifluoromethyl-1*H*-pyrazole (^{125}I -IMTP) and 5-(4-[^{125}I]iodophenyl)-1-[4-(aminosulfonyl)phenyl]-3-trifluoromethyl-1*H*-pyrazole (^{125}I -IATP) [22] were used as reference compounds.

2.6. *In vitro* cell uptake study

Since the conventional murine macrophage-like cell line J774.1 is composed of a heterogeneous mixture of cells, JA-4 cells were subcloned from J774.1 cells to obtain a homogeneous cell population. The culturing of JA-4 cells was performed as described previously [34]. In brief, the cells were maintained and cultured in 10 ml of Ham's F-12 medium (Flow Laboratories, McLean, VA, USA), supplemented with 10% heat-inactivated fetal bovine serum (GIBCO, Grand Island, NY, USA), 50 U/ml of penicillin and 50 mg/ml of streptomycin (Flow Laboratories) in a 100-mm plastic dish (Falcon #1001; Becton Dickinson, Lincoln Park, NJ, USA) at 37°C in a CO₂ incubator (5% CO₂-95% humidified air). In order to induce COX-2, aliquots of the cell suspension were placed into 12-well plates and stimulated with linterfero (LPS, 10 µg/ml) and interferon-γ (IFN-γ, 50 U/ml) for 18 h at 37°C in a humidified atmosphere containing 5% CO₂ and 20% O₂. The stimulated and control cells were washed twice with HEPES-buffered Krebs solution (131 mM NaCl, 5.5 mM KCl, 1 mM MgCl₂, 2.5 mM CaCl₂, 25 mM NaHCO₃, 1 mM NaH₂PO₄, 5.5 mM D-glucose, 20 mM HEPES, pH 7.4). After incubation in HEPES buffer at 37°C for 10 min, ^{125}I -FIMA (37 kBq/ml) was added with nonradioactive FIMA (none and 10⁻⁹ to 10⁻⁵ M in final concentration), and the cells were incubated at 37°C for 60 min and then were washed twice with ice cold phosphate-buffered saline. The cells were lysed with 1% (w/v) sodium dodecyl sulfate and 10 mM sodium tetraborate decahydrate, collected and counted in an auto well gamma counter (Cobra II Auto-Gamma, Packard, Tokyo, Japan). The protein content was determined using a BCA protein assay kit (Thermo Fisher Scientific, Waltham, MA, USA). The uptake levels of ^{125}I -FIMA are expressed as the percentage of incubated dose per mg protein (% dose/mg protein).

2.7. Western blotting

COX-2 expression levels in the stimulated and control macrophage-like cells (JA-4) were examined by Western blotting. Each cell lysate, prepared from the stimulated and control cells, was mixed with a sample buffer (1% sodium dodecyl sulfate, 10% glycerol, 62.5 mM Tris-HCl (pH 6.8), 0.01% bromo phenol blue, 5% 2-mercaptoethanol) and was subjected to electrophoresis on sodium dodecyl sulfate, 5–20% polyacrylamide gel, followed by transfer to a polyvinylidene difluoride membrane. After blocking with Blocking One (03953-95, Nacalai Tesque, Kyoto, Japan), membranes were incubated with the anti-COX-2 antibody (rabbit polyclonal antibody to murine COX-2 amino acids

570-598, Cayman Chemical), followed by horseradish peroxidase-conjugated swine anti-rabbit immunoglobulin antibody. Bands were visualized by the ECL plus Western Blotting Detection System (RPN2132, GE Healthcare UK, Buckinghamshire, England) using a Luminocapture instrument (BIO-RAD Laboratories, Hercules, CA). Immunoblotting for β-actin was used as a protein loading control.

2.8. Animal experiments

Animal studies were conducted in accordance with institutional guidelines, and experimental procedures were approved by the Kyoto University Animal Care Committee.

Biodistribution studies of ^{125}I -FIMA were performed in male Sprague–Dawley rats (280–310 g). ^{125}I -FIMA (74 kBq/rat) was administered to rats under chloral hydrate anesthesia by tail vein injection. At 10, 30, 60 and 180 min after administration, rats were sacrificed by exsanguination under chloral hydrate anesthesia. Blood and organs were excised and weighed, and radioactivity was measured with an auto well gamma counter (ARC2000, Aloka, Tokyo, Japan). Radioactivity levels in the tissues are expressed as the percentage of injected dose per organ (% ID) and/or the percentage of injected dose per gram of tissue (% ID/g).

3. Results

3.1. Synthesis and radiolabeling

FIMA, FTMAM and lumiracoxib were obtained with overall yields of 7.2%, 6.4% and 19.4%, respectively, from the corresponding starting materials. The radiosynthesis of ^{125}I -FIMA was achieved with an electrophilic iododestannylation reaction. ^{125}I -FIMA was obtained with no carrier being added following separation from the precursor (FTMAM) using reverse phase HPLC with a radiochemical yield of 36–51% ($n=3$). The radiochemical purity and specific activity were determined to be greater than 95% ($n=3$) and 47–72 GBq/µmol ($n=3$), respectively.

3.2. COX inhibitory potency

FIMA inhibited COX-2 in a concentration dependent manner, while showing no inhibitory potency for COX-1 in concentrations up to 10⁻⁴ M. Table 1 summarizes the IC₅₀ values of the test compounds. The IC₅₀ value of FIMA was 2.46 µM for COX-2 and 446 µM for COX-1. The COX-2 inhibitory potency of FIMA was higher than that of indomethacin (IC₅₀=20.9 µM) and was comparable to the potencies of lumiracoxib (IC₅₀=0.77 µM) and diclofenac (IC₅₀=0.98 µM). The IC₅₀ ratio (COX-1/COX-2) for FIMA was 182 which is comparable to that of lumiracoxib.

3.3. Distribution coefficients

The distribution coefficient ($\log D_{7.4}$) of ^{125}I -FIMA was 1.84±0.01 ($n=4$) and was less than those of the two radioligands, ^{125}I -IMTP ($\log D_{7.4}$ =3.09±0.11, $n=3$) and

Table 1
COX inhibitory potency and selectivity of FIMA and reference compounds

Compounds	IC ₅₀ (μM)		IC ₅₀ ratio (COX-1/COX-2)
	COX-1	COX-2	
FIMA	446±317	2.46±0.78	182
Lumiracoxib	164±75	0.77±0.21	214
Diclofenac	0.12±0.08	0.98±0.26	0.12
Indomethacin	0.19±0.13	20.9±10.4	0.009

Mean±S.D. for three to four independent experiments.

¹²⁵I-IATP (logD_{7.4}=2.97±0.01, n=4) which were used as reference compounds.

3.4. In vitro cell uptake study

Cell uptake characteristics of ¹²⁵I-FIMA were assessed in control and LPS/IFN-γ-stimulated macrophages (Fig. 4). The accumulation level of ¹²⁵I-FIMA in LPS/IFN-γ-stimulated macrophages was significantly higher than that in control macrophages under conditions without nonradioactive FIMA. The accumulation level of ¹²⁵I-FIMA in LPS/IFN-γ-stimulated macrophages decreased with the addition of nonradioactive FIMA in a concentration dependent manner, while in control macrophages, the accumulation level was unaffected by added nonradioactive FIMA.

Western blot analysis confirmed a significant COX-2 expression in LPS/IFN-γ-stimulated macrophages while no obvious COX-2 expression was observed in control macrophages (Fig. 4B).

3.5. Biodistribution

The biodistribution of ¹²⁵I-FIMA in normal rats is shown in Table 2. Radioactivity in the blood decreased rapidly and the level was 0.08±0.02% ID/g at 180 min after tracer administration. At 10 min after the injection, high levels of radioactivity were found in the liver and kidneys but

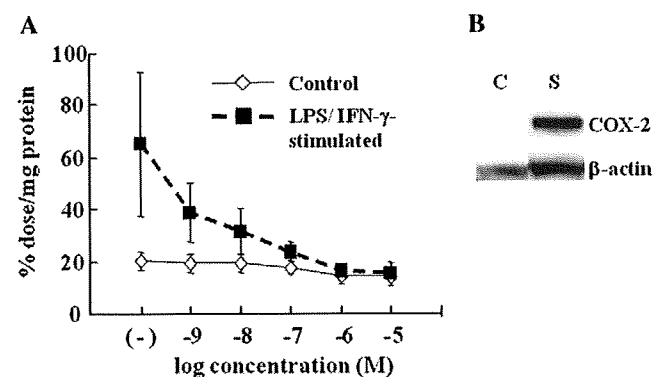


Fig. 4. ¹²⁵I-FIMA accumulation and COX-2 expression in LPS/IFN-γ-stimulated and control macrophages. (A) ¹²⁵I-FIMA and nonradioactive FIMA (0, 10⁻⁹–10⁻⁵ M) were incubated with macrophages for 60 min. Mean±S.D. for four experiments. (B) Western blot analysis of COX-2 expression. C, control; S, LPS/IFN-γ-stimulated macrophages.

Table 2
Biodistribution of ¹²⁵I-FIMA in normal rats

		Time after injection (min)			
		10	30	60	180
Blood	% ID/g	0.55±0.18	0.24±0.02	0.18±0.01	0.08±0.02
Plasma	% ID/g	1.28±0.40	0.57±0.05	0.44±0.05	0.19±0.05
Muscle	% ID/g	0.09±0.03	0.04±0.01	0.03±0.01	0.02±0.00
Heart	% ID/g	0.28±0.10	0.12±0.01	0.08±0.01	0.03±0.01
	% ID	0.24±0.08	0.11±0.01	0.08±0.02	0.03±0.01
Lung	% ID/g	0.36±0.10	0.27±0.19	0.14±0.01	0.07±0.01
	% ID	0.43±0.13	0.38±0.26	0.17±0.02	0.07±0.02
Liver	% ID/g	2.93±1.10	1.04±0.14	0.67±0.05	0.28±0.04
	% ID	25.5±10.4	9.90±0.99	5.88±0.61	2.48±0.35
Kidneys	% ID/g	0.95±0.39	0.81±0.13	0.63±0.09	0.33±0.10
	% ID	2.18±0.87	1.90±0.19	1.49±0.25	0.76±0.23
Pancreas	% ID/g	0.18±0.05	0.10±0.02	0.07±0.01	0.04±0.01
	% ID	0.11±0.06	0.05±0.01	0.03±0.00	0.02±0.01
Spleen	% ID/g	0.14±0.04	0.10±0.05	0.05±0.01	0.03±0.01
	% ID	0.07±0.02	0.05±0.02	0.03±0.00	0.01±0.00
Stomach	% ID/g	0.47±0.19	0.86±0.46	1.28±1.00	0.50±0.27
	% ID	1.00±0.40	1.77±0.97	2.64±1.92	0.95±0.50
Intestine	% ID/g	0.33±0.19	0.46±0.16	0.83±0.14	1.70±0.32
	% ID	4.95±3.08	7.30±3.34	12.16±2.56	22.46±2.39
Brain	% ID/g	0.04±0.02	0.02±0.00	0.02±0.00	0.01±0.00
	% ID	0.08±0.03	0.04±0.00	0.03±0.00	0.01±0.00
Thyroids	% ID/g	1.15±1.06	0.57±0.08	2.28±2.14	6.60±3.58
	% ID	0.01±0.00	0.01±0.00	0.01±0.00	0.03±0.02

Mean±S.D. for five animals.

decreased with time. The radioactivity level in the intestine gradually increased with time and reached 1.70±0.32% ID/g at 180 min. ¹²⁵I-FIMA showed no significant accumulation in the stomach and thyroid, and the maximum accumulation doses in these tissues were 2.64% ID (60 min) and 0.03% ID (180 min), respectively. Significant levels of radioactivity were not found in the brains of rats.

4. Discussion

In this study, we synthesized a radioiodinated lumiracoxib derivative, 2-[(2-Fluoro-6-[¹²⁵I]iodophenyl)amino]-5-methylphenyl-acetic acid (¹²⁵I-FIMA). The potential of radioiodinated FIMA for imaging COX-2 expression was evaluated by in vitro and in vivo experiments. The major findings in this study can be summarized as follows: (1) FIMA had a high inhibitory potency and isoform selectivity for COX-2. (2) ¹²⁵I-FIMA showed a significantly higher accumulation in COX-2 induced macrophages than in control macrophages, which decreased with the addition of nonradioactive FIMA in a concentration dependent manner. (3) The biodistribution study in normal rats showed rapid clearance of ¹²⁵I-FIMA from the blood and most organs without significant in vivo deiodination of ¹²⁵I-FIMA. These results indicate radiolabeled lumiracoxib derivatives have the potential to be PET/SPECT tracers of COX-2 expression. Affinity and specificity including isoform selectivity for COX-2 are indispensable prerequisites of PET/SPECT tracers for imaging the enzyme.